JPL PUBLICATION 85-77

Chemistry of MOS-LSI Radiation Hardening

Final Report

Prepared by:
P.J. Grunthaner

(NASA-CR-176651) CHEMISTRY OF MOS-LSI RADIATION HARDENING Final Report (Jet Propulsion Lab.) 88 p HC A05/MF A01
N86-21636
CSCL 07D
Unclas
G3/25 05858

August 15, 1985

Prepared for
Defense Nuclear Agency
Through an agreement with
National Aeronautics and Space Administration
by
Jet Propulsion Laboratory
California Institute of Technology
Pasadena, California

TECHNICAL REPORT STANDARD TITLE PAGE

1. Report No.
JPL Publication 85-77

2. Government Accession No.

3. Recipient's Catalog No.

4. Title and Subtitle
Chemistry of MOS-LSI Radiation Hardening
Final Report

5. Report Date
August 15, 1985

6. Performing Organization Code

7. Author(s)
Prepared by P.J. Grunthaner

8. Performing Organization Report No.

9. Performing Organization Name and Address
JET PROPULSION LABORATORY
California Institute of Technology
4800 Oak Grove Drive
Pasadena, California 91109

10. Work Unit No.

11. Contract or Grant No.
NAS7-918

13. Type of Report and Period Covered
JPL Publication

12. Sponsoring Agency Name and Address
NATIONAL AERONAUTICS AND SPACE ADMINISTRATION
Washington, D.C. 20546

14. Sponsoring Agency Code
RE156 BK-506-54-15-39-0

15. Supplementary Notes

16. Abstract

This task augments an overall effort directed towards achieving qualified sources of MOS-LSI structures that are generically hardened towards total dose radiation.

The objective of this task was to obtain chemical information on MOS test samples. Toward this end, high resolution X-ray photoemission spectroscopy (XPS) has been the primary technique used to characterize the chemistry and structure of the SiO_2/Si interface for a variety of MOS structures with differing degrees of susceptibility to damage by ionizing radiation.

The major accomplishments of this program are (i) the identification of a structurally distinct region of SiO_2 in the near-interfacial region of thermal SiO_2 on Si; (ii) the identification in the near-interfacial region of SiO_2 structural differences between radiation hard and soft gate oxides; (iii) the direct observation of radiation-induced damage sites in thermal SiO_2 with XPS using in situ electron stress; (iv) the correlation of suboxide state distributions at the SiO_2/ Si interface with processing parameters and radiation susceptibility; (v) the development of a chemical mechanism for radiation-induced interface state generation in SiO_2/Si structures and (vi) the development of benign chemical profiling techniques which permit the investigation of oxide/semiconductor structures using surface sensitive electron spectroscopic techniques

17. Key Words (Selected by Author(s))
Electronics and Electrical Engineering
Physical Chemistry
Materials (General)

18. Distribution Statement
Unclassified - Unlimited

19. Security Classif. (of this report)
Unclassified

20. Security Classif. (of this page)
Unclassified

21. No. of Pages
78

22. Price

JPL PUBLICATION 85-77

Chemistry of MOS-LSI Radiation Hardening

Final Report

Prepared by:
P.J. Grunthaner

August 15, 1985

Prepared for
Defense Nuclear Agency
Through an agreement with
National Aeronautics and Space Administration
by
Jet Propulsion Laboratory
California Institute of Technology
Pasadena, California

The research described in this publication was carried out by the Jet Propulsion Laboratory, California Institute of Technology, and was sponsored by the National Aeronautics and Space Administration and the Defense Nuclear Agency.

ABSTRACT

This task augments an overall effort at the National Aeronautics and Space Administration (NASA) and the Defense Nuclear Agency (DNA) directed towards achieving qualified sources of MOS-LSI structures that are generically hardened towards total dose radiation. The work reported here covers research performed at the Jet Propulsion Laboratory during the period 15 April 1981 to 15 April 1983, except where noted in the introduction. This effort was supported primarily under a NASA - Office of Aeronautics and Space Technology (OAST) program with additional support provided by DNA (JPL Task Plan No. 80-1494) through Dr. James McGarrity of the Harry Diamond Laboratory.

The objective of this task was to obtain chemical information on MOS test samples fabricated at Sandia Laboratories and electrically characterized at Harry Diamond Laboratory and Northrup Research Center. Toward this end, high resolution X-ray photoemission spectroscopy (XPS) has been the primary technique used to characterize the chemistry and structure of the SiO_2/Si interface for a variety of MOS structures with differing degrees of susceptibility to damage by ionizing radiation.

The major accomplishments of this program are (i) the identification of a structurally distinct region of SiO_2 in the near-interfacial region of thermal SiO_2 on Si; (ii) the identification in the near-interfacial region of SiO_2 structural differences between radiation hard and soft gate oxides; (iii) the direct observation of radiation-induced damage sites in thermal SiO_2 with XPS using *in situ* electron stress; (iv) the correlation of suboxide state distributions at the SiO_2/Si interface with processing parameters and radiation susceptibility; (v) the development of a

chemical mechanism for radiation-induced interface state generation in SiO_2/Si structures and (vi) the development of benign chemical profiling techniques which permit the investigation of oxide/semiconductor structures using surface sensitive electron spectroscopic techniques.

The contributors to this work include the following personnel:

Mr. Charles Aker
Ms. Cindy Butler
Dr. Phrosty Chimilikis
Dr. Frank J. Grunthaner
Dr. Paula J. Grunthaner
Dr. Michael H. Hecht
Mr. Don Lawson
Dr. Blair F. Lewis
Dr. Anupam Madhukar
Dr. Joseph Maserjian
Mr. Richard Vasquez
Dr. James Wurzbach
Ms. Pat Zajicek

TABLE OF CONTENTS

I. INTRODUCTION 1

II. EXPERIMENTAL 3

A. Sandia Sample Matrix 3
B. X-ray Photoemission Spectrometer 3
C. Chemical Profiling 4
D. Removal of the Al and Polysilicon Gate Electrode 7

III. CHEMICAL STRUCTURE OF THE SiO_2/Si INTERFACE: THE NEAR-INTERFACIAL REGION 11

A. Evidence for a Structurally Distinct Region of SiO_2 11

1. Analysis of Core Level Binding Energies 11
2. Analysis of Core Level Intensities 21
3. Chemical Etch Rates 30
4. SEXAFS 30

B. Comparison of Hard and Soft Gate Oxides 32

IV. *IN-SITU* ELECTRON STRESS EXPERIMENTS 39

A. Introduction 39
B. Oxide Thickness and Temperature Dependence 42
C. Model for Radiation-Induced Bond Cleavage 42

V. BOND STRAIN GRADIENT MECHANISM FOR RADIATION INDUCED INTERFACE STATE GENERATION 45

A. The Model 45

1. Step 1: Radiation -Induced Cleavage of a Si-O Covalent Bond 47
2. Step 2: Hydroxyl Assisted Migration of the Non-bridging Oxygen Defect 47
3. Step 3: Formation of Amphoteric Traps at the SiO_2/Si Interface 51
4. Relationship of Model to Other Observations 53

VI. THE CHEMICAL STRUCTURE OF THE SiO_2/Si INTERFACE: THE SiO_x TRANSITION LAYER 54

- A. Localization of Suboxide States at the SiO_2/Si Interface 56
- B. Crystallographic Dependence and Interfacial Roughness 61
- C. Process Dependence: Post-Oxidation Anneal Temperature 65
- D. Implications for the BSG Mechanism 67

VII. CONCLUSIONS 69

VIII. RECOMMENDATIONS 73

IX. REFERENCES 77

TABLE

TABLE 1: Si-O-Si bond angle, Si-O bond distance, number of tetrahedrons per ring for various polymorphs of SiO_2 18

LIST OF ILLUSTRATIONS

Page

Figure 1: Sequential wide scan XPS spectra taken at each step of a chemical depth profile of a thermal oxide grown on Si(100)........................ 6

Figure 2: Schematic of XeF_2 gas phase etching apparatus.............................. 8

Figure 3: Si 2p spectra illustrating the removal of a thick (8500 Å) polysilicon gate electrode from a thermal gate oxide..10

Figure 4: Typical Si 2p core level spectra for a chemical depth profile of a thermal oxide, showing relative intensities of the oxide and substrate contributions.. 12

Figure 5: Si 2p core level spectra for a 41 Å thermal oxide, recorded as a function of increasing flood-gun voltages...13

Figure 6: Plot of the full width at half maximum (FWHM) of the Si 2p oxide peak versus the apparent chemical shift of the oxide line relative to that of the substrate line...15

Figure 7: Illustration of the flexible Si-O-Si bond angle linking SiO_4 tetrahedron units in SiO_2.. 16

Figure 8: Schematic of the ring network in a hypothetical A_2O_3 glass network.. 18

Figure 9: The silicon-to-oxygen fractional charge transfer per bond as a function of the Si-O-Si bridging bond angle.................................. 19

Figure 10: (a) Schematic illustrating the layer approximation used in the Dλ calculation. (b) A Dλ profile for a thermal oxide on Si(100) and a deposited CVD oxide...22

Figure 11: Schematic illustration of "profiles" obtained using (a) fixed photon energy photoemission in conjunction with chemical profiling techniques and (b) variable photon energy photoemission.. 25

Figure 12: Si 1s spectra from a 53 Å thermal oxide taken at photon energies 1950 (top), 2000, 2050, 2100, and every 100 to 3700 eV.. 26

Figure 13: Substrate-oxide Si 1s peak separation as a function of electron kinetic energy.......27

Figure 14: The average Dλ product versus kinetic energy for a thermal oxide on Si (100).......29

Figure 15: Plot of the oxide removal rate as a function of oxide thickness for radiation hard and soft gate oxides.......31

Figure 16: Surface extended X-ray absorption fine structure (SEXAFS) spectra after transform to momentum space and background subtraction.......33

Figure 17: Fourier transform of the spectra in figure 16.......34

Figure 18: Plot of the Dλ product as a function of oxide thickness for radiation hard and soft pyrogenic gate oxides.......36

Figure 19: Plot of the average Dλ product versus kinetic energy for an 18 Å radiation soft oxide and for 11 Å and 53 Å radiation hard oxides.......38

Figure 20: Plot of the sequential decay of Si 2p spectra (A to D) for a nominally radiation hard gate oxide after 10 eV electron irradiation under UHV conditions.......41

Figure 21: Illustration of the radiation-induced cleavage of a strained Si-O covalent bond in the SiO_2 network.......43

Figure 22: Summary of the proposed three-stage bond strain gradient mechanism for the formation of interface states following exposure of an oxide to ionizing radiation.......46

Figure 23: Schematic representation of defect propagation for the growth of quartz crystals in fused silica.......49

Figure 24: Illustration of step 2 of the proposed three-stage bond strain gradient mechanism, demonstrating the OH assisted migration of the non-bridging oxygen defect.......50

Figure 25: Schematic of step 3 of the proposed three-stage bond strain gradient mechanism, illustrating the formation of amphoteric traps at the SiO_2/Si interface.......52

Figure 26: Illustration of the five possible oxidation states of silicon 55

Figure 27: (a) upper curve: the Si 2p region of a thin thermal oxide on silicon; lower curve: data from upper curve with the spin-orbit components removed. Si 2p spectra from bulk Si and SiO_2 are overplotted to emphasize the suboxide region (shaded). (b) Difference spectrum 57

Figure 28: Normalized Si 2p intensities of the oxide and suboxide components plotted against a reduced average oxide thickness for a chemcial depth profile of a thermal oxide on Si (100) 59

Figure 29: Expansion of the vertical scale in figure 28, emphasizing the suboxide contributions 60

Figure 30: Idealized diagram of local atomic interface geometry 62

Figure 31: Normalized Si 2p suboxide intensities versus a reduced average oxide thickness for a dry thermal oxide on Si (111) 63

Figure 32: Normalized Si 2p suboxide intensities versus a reduced average oxide thickness for a dry thermal oxide on Si (100) 64

Figure 33: Summary of suboxide intensities for a pyrogenic thermal oxide (850 Å thick) comparing the effect of a 1150° C post-oxidation anneal versus no anneal 66

Figure 34: Schematic of the reaction between a non-bridging oxygen defect and a Si^{+3} site at the SiO_2/Si interface 68

I. INTRODUCTION

The deleterious effect of ionizing radiation and hot electrons on the gate dielectric of MOS structures is a reliability problem of great significance. Such phenomena are known to produce interface states and fixed positive charge in the gate dielectric, giving rise to threshold voltage shifts and degradation of the transconductance. The goal of this task was to examine how structural and chemical defects in the gate dielectric are related to such electrically important phenomena as interface states, electron and hole traps, and fixed charge. In particular, our objective was to use high-resolution X-ray photoemission spectroscopy (XPS) to obtain chemical information on MOS test structures fabricated at Sandia Laboratories and electrically characterized at Harry Diamond Laboratory and Northrup Research Center. The results of this research are summarized in this final report.

This report is organized as follows: In section II, the experimental details of sample handling and subsequent XPS analysis are presented. Section III is devoted to the experimental evidence we have accumulated for the existence of a structurally distinct region of SiO_2 near the SiO_2/Si interface, with particular emphasis placed on the structural differences between radiation hard and soft oxides in this region. Work is presented utilizing not only fixed photon energy XPS, but variable photon energy photoemission and surface extended X-ray absorption fine structure (SEXAFS) as well. Not all of this work was performed during the existence of the DNA contract. The variable photon energy photoemission and SEXAFS studies were performed under NASA support after the expiration of the DNA contract, but utilized the samples provided by Sandia Laboratory. The results of these experiments have therefore been included for completeness. Section IV summarizes results from *in situ* electron irradiation experiments devised to examine the effect of ionizing radiation on the network structure of SiO_2. The results from sections III and IV are combined in section V to provide the basis for a chemical mechanism for the radiation-induced formation of interface states in SiO_2/Si structures. Finally, in section VI, our recent results on the structure of the monolayer SiO_x transition layer between SiO_2 and the Si substrate are discussed with a view towards understanding how atomic roughness at the interface is related to the susceptibility of a SiO_2/Si structure to radiation damage. Some of the work in this section was also performed after the expiration of the DNA contract, but once again utilized samples from the original Sandia matrix.

The details of the work described here may be found in the following publications:

F. J. Grunthaner, B. F. Lewis, J. Maserjian, and A. Madhukar, J. Vac. Sci. Technol., 20, 747 (1982)

F. J. Grunthaner, P. J. Grunthaner, and J. Maserjian, IEEE Trans. Nuclear Sci., NS-29, 1462 (1982)

M. H. Hecht, F. J. Grunthaner, P. Pianetta, L. I. Johansson, and I. Lindau, J. Vac. Sci. Technol., A2, 584 (1984)

M. H. Hecht, P. J. Grunthaner, and F. J. Grunthaner, Proceedings of the 17th International Conference on the Physics of Semiconductors, J. D. Chadi and W. A. Harrison, eds., (Springer-Verlag, New York, 1985), p 217

M. H. Hecht and F. J. Grunthaner, proceedings for the Society of Photo-Optical Engineers (SPIE) conference, Spectroscopic Characterization Techniques for Semiconductor Technology II, vol. 24, F. H. Pollak, ed., 1985, p 18

II. EXPERIMENTAL

II.A. Sandia Sample Matrix

The MOS test samples studied in this task were fabricated at Sandia Laboratories under the direction of Dr. Paul V. Dressendorfer and were specifically designed to isolate key process requirements for radiation hard MOS device structures. All structures were fabricated on n-type silicon with (100) orientation. Radiation hard pyrogenic oxides were grown at 900^{o} C to a thickness of approximately 700-800 Å, while hard dry oxides were grown at 1000^{o} C to similar thicknesses. Radiation soft gate oxides were prepared from hard gate oxides by an additional anneal in dry N_2 at 1150^{o} C for 30 minutes. Both Al and polysilicon gate structures were examined. Structures utilizing an Al gate electrode were annealed to 450^{o} C in nitrogen for 30 minutes after metallization. For polysilicon gate samples, polysilicon was first deposited (approximately 8500 Å) and doped, followed by the deposition of a CVD oxide, as would occur in a full polysilicon gate device process. The CVD oxide was removed by Sandia Laboratory prior to shipping to JPL using a buffered HF solution. Samples received at JPL were stored under dry nitrogen until examined.

II.B. X-ray Photoemission Spectrometer

The X-ray photoemission spectrometer used in these studies is a modified HP5950A ESCA spectrometer. Sample preparation is performed in a stainless-steel dry box continuously flushed with nitrogen gas generated from a liquid nitrogen source and connected to the sample introduction port of the spectrometer. For most of the experiments reported here the spectrometer was operated at 0.4-0.5 eV resolution and at a base pressure of less than 5×10^{-10} torr.

The spectrometer is equipped with a monochromatic X-ray source (1486.6 eV photon energy) which irradiates the sample at a dose rate of less than 10^{-5} rad-Si/hour. There is also available a low energy electron gun capable of irradiating the sample with electrons of kinetic energy between 0 and 10 eV at currents up to 1 milliamp.

II.C. Chemical Profiling

X-ray photoemission, like many other electron spectroscopies, is characterized by a sensitivity established predominantly by the mean free path of the photo-emitted electrons. Since the mean free path is defined as the depth at which the signal intensity from an emitting species has been attenuated by 1/e, chemical species as far below the surface as 2 to 3 times the electron mean free path can still be detected with reasonable signal-to-noise statistics. For electrons emitted from the Si 2p core level of elemental Si and SiO_2 using an incident photon energy of 1486.6 eV, the mean free path is approximately 26 Å and 40 Å, respectively. This restricts the observation depth for this system to less than 100 Å of SiO_2 on Si. To study the SiO_2/Si interface of a typical device gate oxide (approximately 1000 Å SiO_2), the oxide must therefore be physically thinned by some means.

Overlayers are typically thinned using either ion sputtering or chemical etching. In our laboratory we have chosen to use chemical etching exclusively since considerable evidence exists in the literature regarding the chemical damage imparted by ion sputtering techniques. Specifically with regard to the SiO_2/Si system, it has been demonstrated that Ar^+ ion sputtering of thermally grown SiO_2 on Si induces chemical damage as evidenced by the formation of intermediate oxidation states of Si.[1] Chemical thinning of the oxide can likewise leave a chemically damaged region, but studies conducted in our laboratory indicate that this damaged region is limited to the first few surface layers of the oxide. The relatively long electron mean free paths observed in XPS allow one to look beyond this damaged region to examine the buried interfacial region.

The chemical profiling of SiO_2/Si structures was performed in a nitrogen-flushed dry box connected to the sample introduction chamber of the XPS. Samples were scribed and cleaved to 9.5 x 9.5 mm squares and mounted on a Teflon sample holder attached to a high speed synchronous motor. The samples were spun at 3600 to 12000 rpm while a solution of 10% HF in pharmaceutical grade absolute ethanol was added in controlled increments (generally 100 to 200 microliters per etch step). The sample was rinsed with ethanol using the same technique. We have found this spinning technique to be far superior to simple immersion of the sample in an etchant solution for a number of reasons. First, the etch rate can be precisely controlled by varying the etchant concentration, the volume of etchant used, and the sample rpm. Second, the etch rate is uniform over the sample area. After etching an 800 Å oxide to 100 Å, ellipsometric measurements over the sample area indicate a variation in the oxide thickness of only a few angstroms. Third, the act of spinning the sample while etchants and rinse solutions are added minimizes contamination residues on the sample surface. We consistently find that samples which have been spin-etched show lower carbon and fluorine contamination than samples etched via immersion.

After chemical etching, the sample is immediately introduced into the ultra-high vacuum (UHV) environment of the XPS spectrometer. Typical times required between sample mounting and introduction into the vacuum chamber are on the order of several minutes. Figure 1 shows XPS survey spectra obtained during a typical chemical profile by spin-etching a SiO_2/Si sample at 3600 rpm with 10% HF in absolute ethanol. Notice that the carbon 1s core level is not detectable

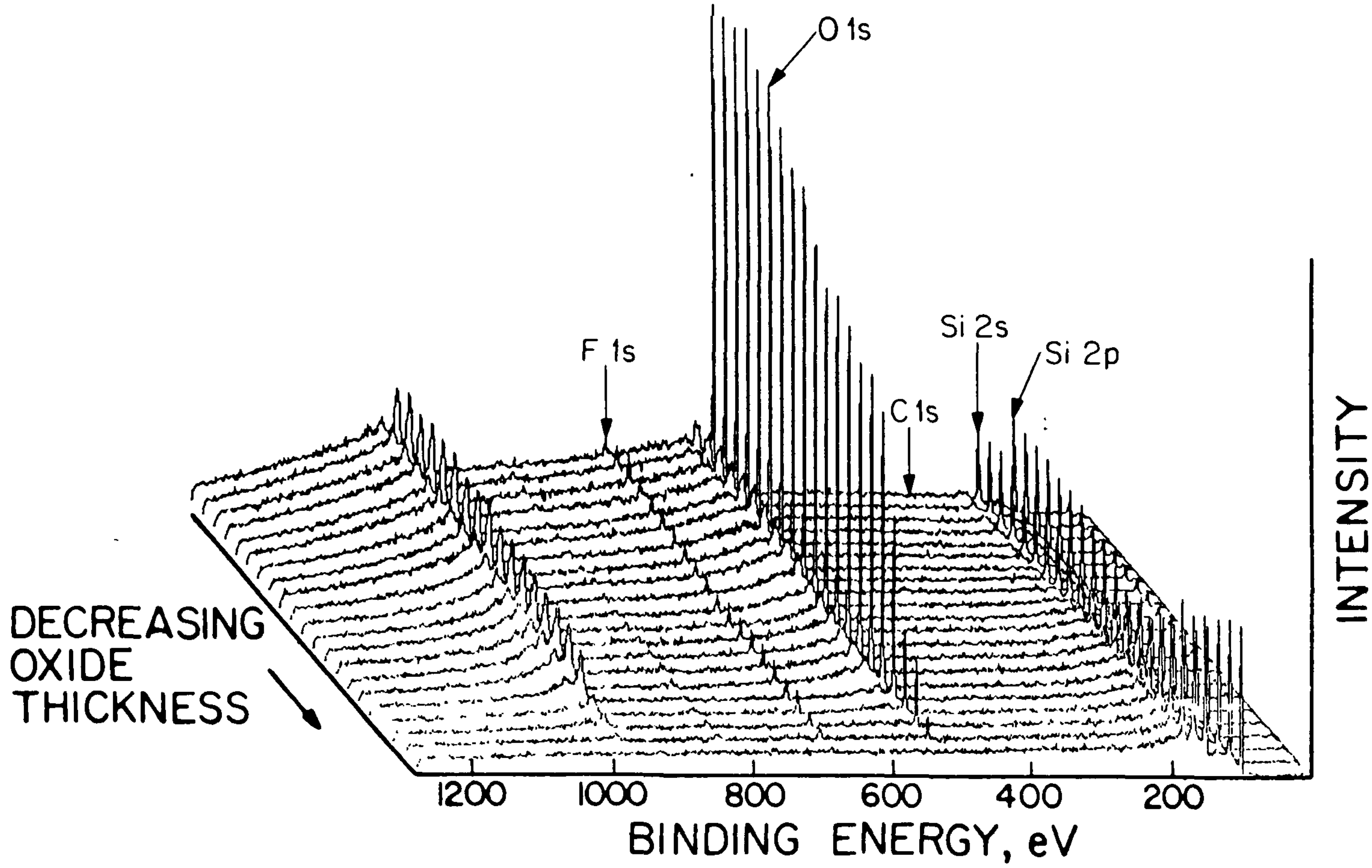

Figure 1: Sequential wide scan XPS spectra taken at each step of a chemical depth profile of a thermal oxide grown on Si (100). Energy positions of appropriate core levels are indicated.

at any point during the profile, indicating that neglible carbon contamination occurs during the etch steps. The only impurity detected is that of fluorine, which is an etchant residue remaining on the oxide surface.

II.D. Removal of the Al and Polysilicon Gate Electrode

The majority of samples in the Sandia matrix have either Al or polysilicon deposited on the gate oxide. In order to spectroscopically examine the oxide structure, these metallic overlayers must be removed without disturbing the underlying oxide. Our initial attempts utilized conventional chemical etches to remove the Al and polysilicon, but with limited success. As discussed below, considerable effort was expended in developing benign techniques for the removal of these gate electrodes.

Initially, the polysilicon gate material was removed using the conventional chemical etch often used in industry for polysilicon removal which consists of a 1:100:10:50 solution of HF, HNO_3, CH_3CO_2H, and H_2O. This etchant, which etches SiO_2 as well as polysilicon, left an unacceptable nonuniform oxide with thickness variations greater than 10 Å. In some cases, XPS analysis of treated samples indicated that not all of the polysilicon was removed by the etch, even following repeated exposures of the samples to the etchant solution. Subsequent SEM studies of these samples showed the presence of small islands of polysilicon that resisted reaction with the etchant.

To circumvent the above problems, a gas phase XeF_2 etching system was implemented as diagrammed in figure 2. XeF_2 is a solid with a vapor pressure of approximately 4.5 torr at room temperature. Gaseous XeF_2 will etch crystalline and polycrystalline Si, but it is inert towards SiO_2. The mechanism for this gas phase etching is discussed extensively in the literature.[2,3] As diagrammed in figure 2, the

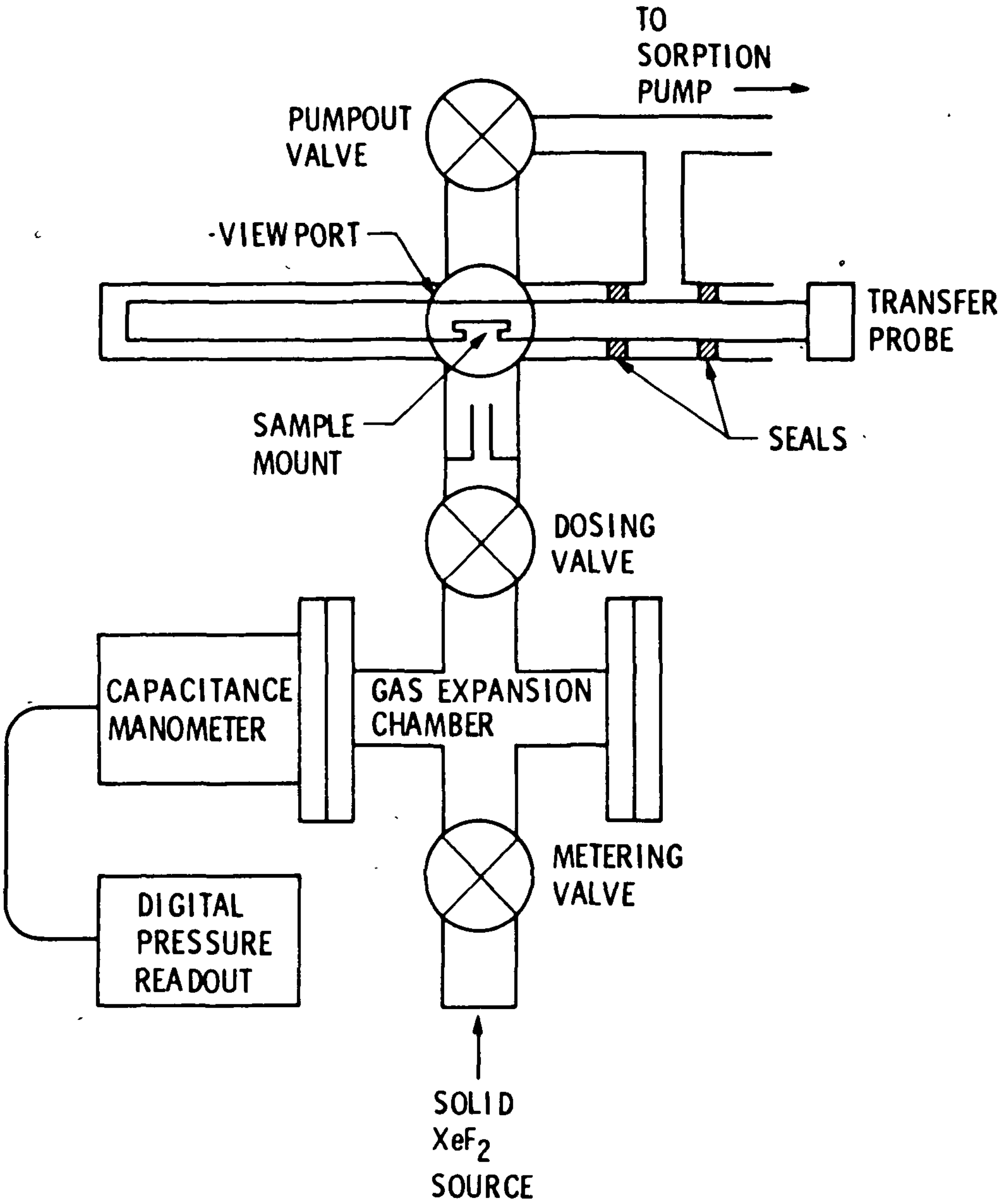

Figure 2: Schematic of XeF_2 gas phase etching apparatus.

sample chamber is evacuated to approximately 1 millitorr and the XeF_2 is allowed to sublime into the chamber. After several hours of exposure to the reactive gas, the polysilicon overlayer is completely removed, as demonstrated by Si 2p spectra obtained before and after exposure (figure 3). Although the efficiency of the XeF_2 etchant is approximately 1% per molecular collision,[2,3] subsequent effort in this laboratory has effectively increased this efficiency to 40% by balancing molecular flows and pressure such that each XeF_2 molecule experiences many collisions.[4]

Removing the Al gate electrode prior to examining the gate oxide proved to be a problem that likewise demanded special attention. Conventional solution etches involving various combinations of HNO_3, H_3PO_4, HCl and other acids left a nonuniform oxide surface. A solution to the problem was derived from the knowledge that KOH and NaOH dissolve Al readily, probably via the following reaction:

$$3Al + 2OH^- + 6H_2O \rightarrow 2Al(OH)_4^- + 3H_2$$

To avoid contamination from such small counterions as Na^+ and K^+, several weak bases with counterions too large to penetrate the oxide were investigated. It was found that immersion of a $Al/SiO_2/Si$ structure in a room temperature solution of tetramethyl ammonium hydroxide or tetrabutyl ammonium hydroxide would remove the Al overlayer without perturbing the underlying oxide.

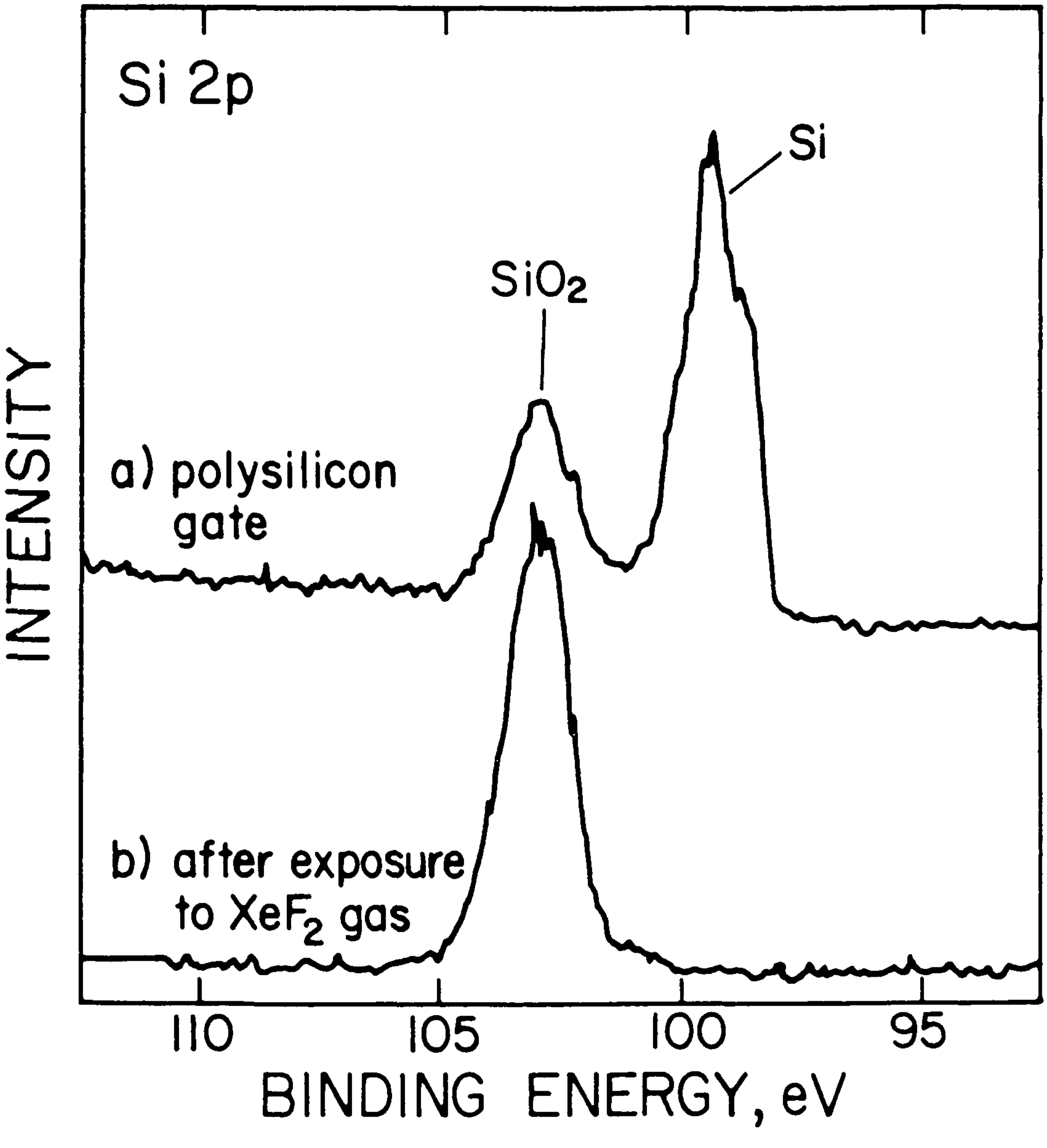

Figure 3: Si 2p spectra illustrating the removal of a thick (8500 Å) polysilicon gate electrode from a thermal gate oxide. In the top panel, the SiO_2 signal corresponds to the native oxide present on the surface of the polysilicon. In the lower panel, the SiO_2 signal corresponds to the thermal oxide under the polysilicon which has been removed by reaction with the XeF_2.

III. CHEMICAL STRUCTURE OF THE SiO_2/Si INTERFACE: THE NEAR INTERFACIAL REGION

III.A. Evidence for a Structurally Distinct Region of SiO_2

III.A.1. Analysis of Core Level Binding Energies

A typical set of Si 2p core level spectra obtained as a function of decreasing oxide thickness is shown in figure 4. The doublet structure at 99.4 eV is due to electrons photoejected from the Si substrate. The broader signal at 104 eV is due to electrons emitted from the SiO_2. As the oxide thickness decreases, the oxide peak begins to shift towards lower binding energy beginning at approximately 50 Å SiO_2. Since the oxide is known to be stoichiometric SiO_2 up to within approximately one monolayer of the SiO_2/Si interface,[6] we have interpreted this shift in terms of changes in the local bonding geometry of SiO_2. Specifically, we suggest that the distribution of Si-O-Si bond angles within the SiO_2 network is different in the near-interfacial region as compared to bulk SiO_2.

Before concluding that the observed binding energy shift of the Si 2p oxide line is due to a change in the local bonding geometry of the SiO_2, one must rule out the possibility that the oxide shift is not due to charging phenomena. The presence of positive or negative charge on the oxide surface changes the surface potential, which causes a shift in the oxide signal relative to the substrate signal. In addition the oxide signal will broaden because such surface charge will give rise to a potential gradient across the oxide. Figure 5 illustrates the apparent energy shift and broadening of the oxide signal as increasing amounts of negative charge are placed on a 41 Å oxide surface using an *in-situ* electron source. It is clear that the observed chemical shift between the Si substrate and oxide signals will depend strongly upon the steady-state charge that has built up on the oxide surface during

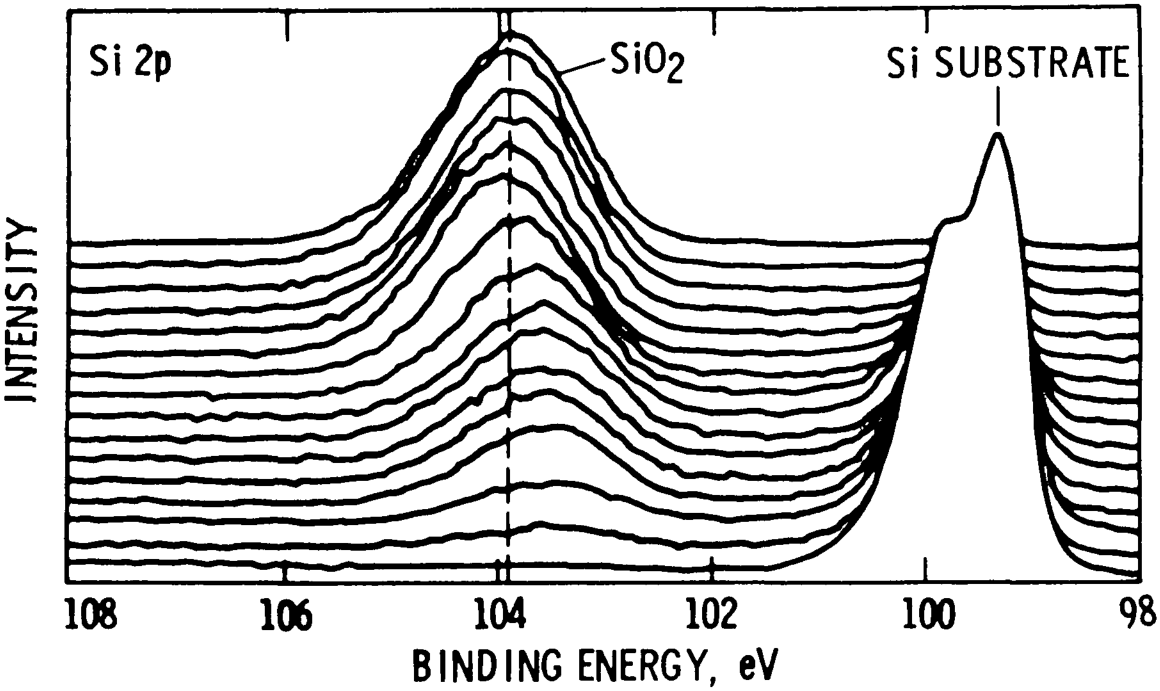

Figure 4: Typical Si 2p core level spectra for a chemical depth profile of a thermal oxide, showing the relative intensities of the oxide and substrate contributions.

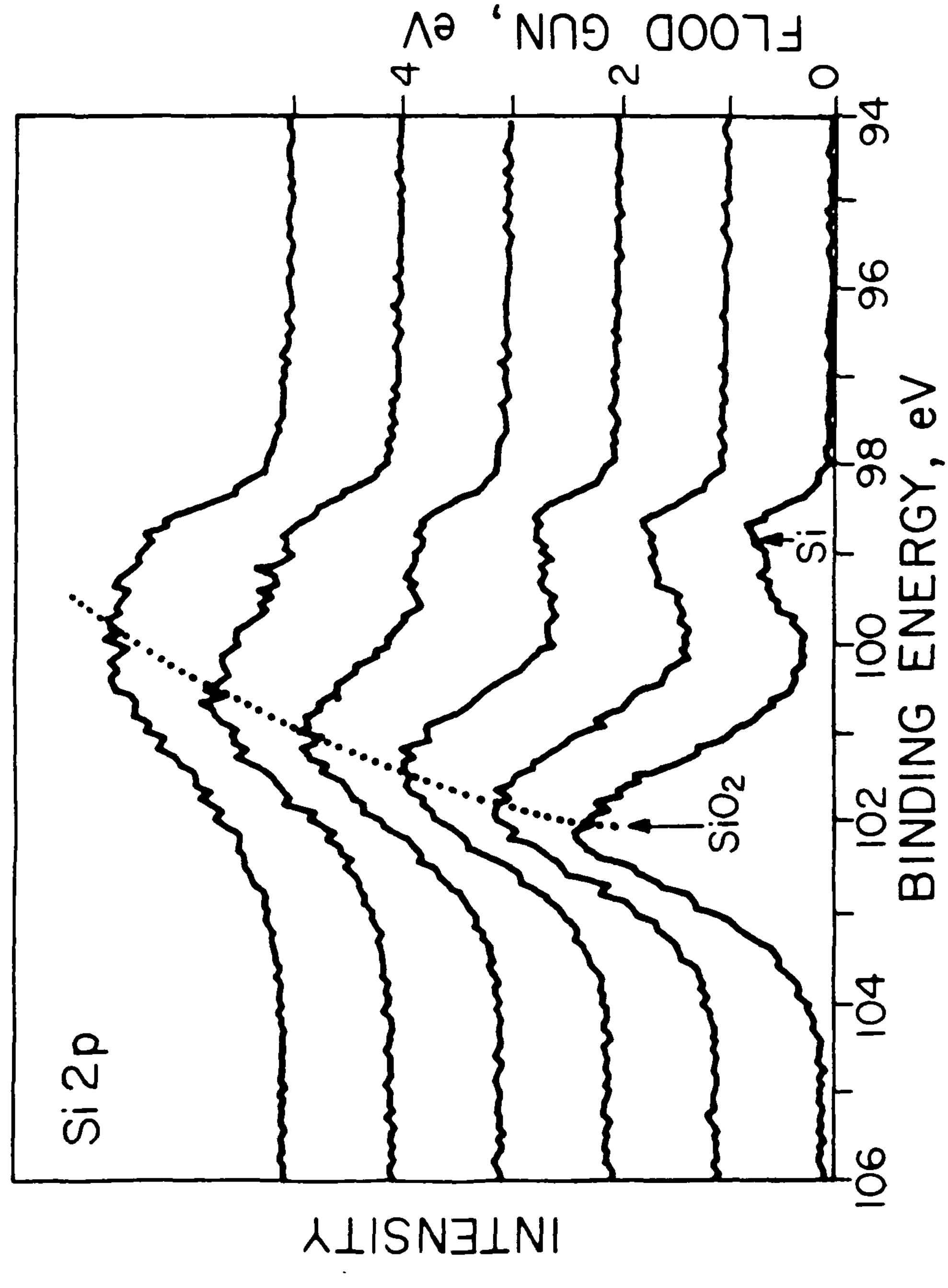

Figure 5: Si 2p core level spectra for a 41 Å thermal oxide, recorded as a function of increasing flood-gun voltages.

the photoemission experiment. The true chemical shift can be obtained only under conditions wherein the charge on the oxide surface is zero, corresponding to a flatband condition with no potential gradient through the oxide. This flatband condition will result in the narrowest oxide signal linewidth and, consequently, by monitoring the width of the oxide line as a function of the electron-induced bias on the oxide surface, one can obtain the true chemical shift. This has been done for 49 Å, 23 Å, and 6 Å oxide films as shown in figure 6. For the 49 Å oxide, there is a clear minimum in the width of the oxide signal, corresponding to a chemical shift of 4.4 eV between the oxide and substrate peaks. For the 23 Å oxide, the curve in figure 6 has broadened considerably, but the minimum in the oxide signal width clearly corresponds to a smaller chemical shift between the oxide and substrate signals. For the 6 Å oxide, the oxide peak could be shifted only a few tenths of an electron volt, indicating that the oxide surface would not stabilize any significant charge. This is not surprising since a barrier only 6 Å wide permits rapid tunneling of charge between the oxide surface and the substrate. The chemical shift between the oxide and substrate peaks for the 6 Å oxide was found to be approximately 4.0 eV, which is smaller than that observed for the 49 Å and 23 Å films. These results indicate that the shift in the oxide signal observed for very thin oxides (see figure 4) is not due to a change in the oxide surface potential as the oxide is thinned. We suggest that a change in the local bonding geometry of the SiO_2 network is responsible for the observed shift. This is explained in greater detail below.

The various polymorphs of SiO_2 are known to consist of SiO_4 tetrahedrons linked together by shared oxygen atoms. Although the O-Si-O bond angle formed within any given SiO_4 tetrahedron is constrained to 109.5^o, the Si-O-Si bridging bond angle, diagrammed in figure 7, can vary over a large range. For example, in

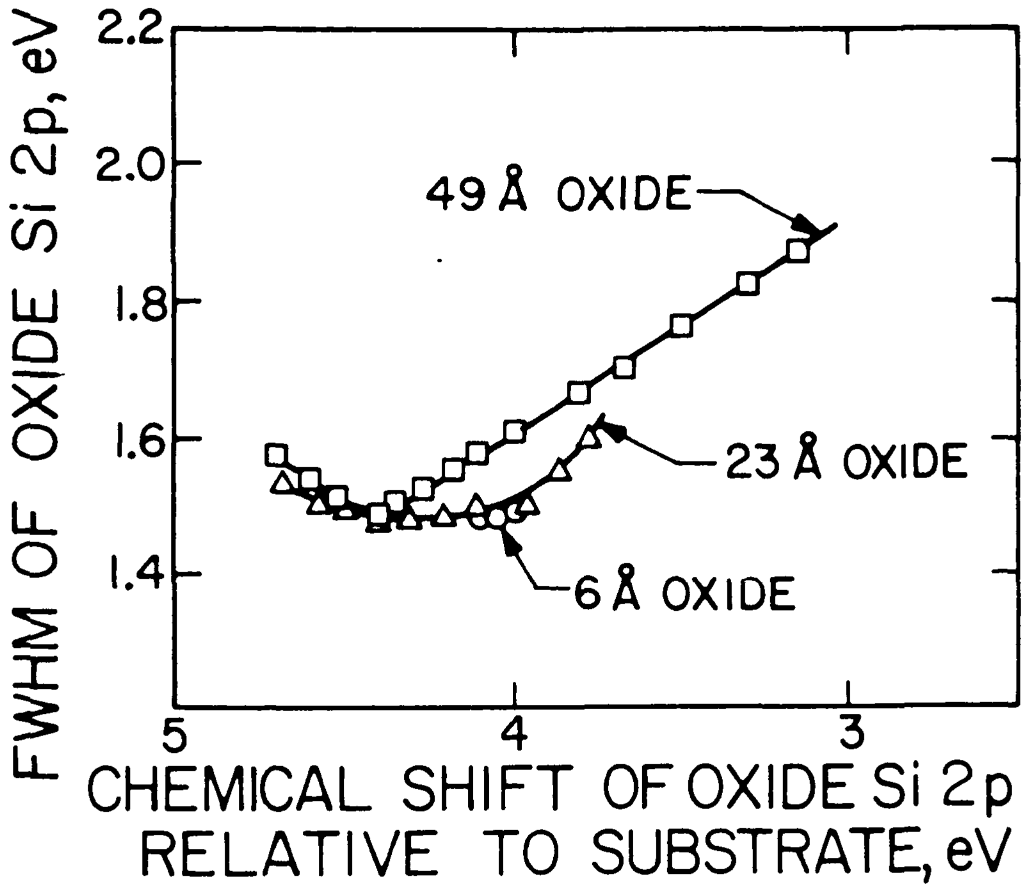

Figure 6: Plot of the full width at half maximum (FWHM) of the Si 2p oxide peak versus the apparent chemical shift of the oxide line relative to that of the substrate line.

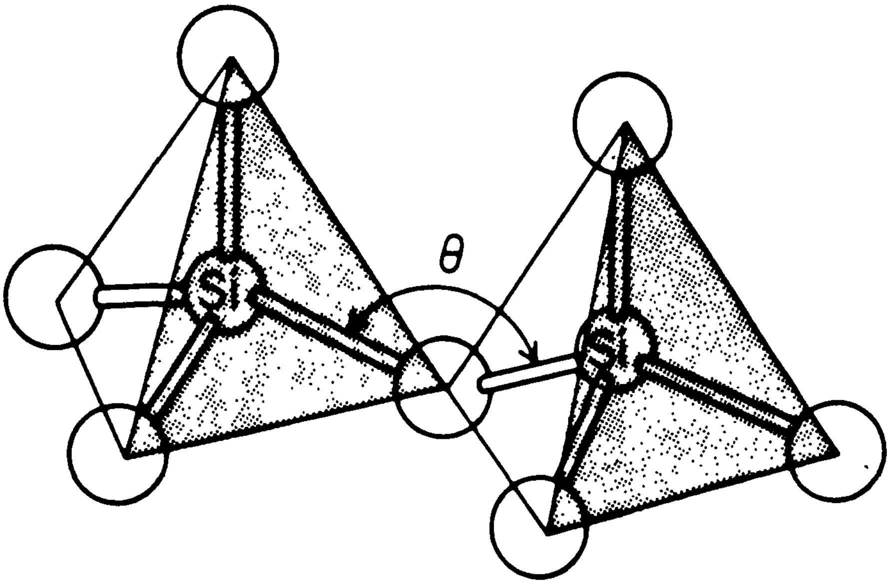

Figure 7: · Illustration of the flexible Si-O-Si bond angle linking SiO_4 tetrahedron units in SiO_2.

the crystalline SiO_2 polymorph α-quartz, this bond angle is 144°, but, as shown in table I, the Si-O-Si bond angle has been found to be as small as 120° (in the mineral coesite) and as large as 168-180° (in the high temperature phase of the mineral cristobalite). In amorphous SiO_2, the full range of Si-O-Si bond angles linking the SiO_4 tetrahedrons is possible. The result is an interconnecting ring system of three to eight SiO_4 tetrahedral units joined via bridging oxygen atoms,[5] as per the Zachariasen network glass model illustrated in figure 8.

X-ray photoemission is sensitive to this variation in the Si-O-Si bridging bond angle because any perturbation in the valence charge distribution of an atom will result in a shift of its core level binding energies. In earlier work, we interpreted core level shifts by means of a structure-induced charge transfer model, utilizing empirical tight binding calculations to relate bridging bond angle and the observed chemical shifts.[6] The results of these calculations are shown in figure 9a and indicate that the smaller the bridging bond angle, the more charge is shifted towards the Si atom, and, hence, the lower the observed Si 2p binding energy. Refinement in the understanding of network glass systems over the years has shown that a change in the bridging bond angle not only affects the charge transfer between the Si and O atoms, but also involves changes in the Si-O bond length and orbital hybridization. This is illustrated in figure 9b using experimental data for the high pressure silica polymorph coesite. Specifically, the oxygen 2s contribution and the Si-O bond length both decrease with increasing Si-O-Si bond angle. This is conceptually easy to grasp if one recalls that electrons are closer to the nucleus for s as compared to p orbitals. Thus, as more s character is added to the bond with increasing bond angle, the effective radius of the bridging oxygen should decrease and the bond length should shorten. An understanding of the precise relationship between the observed photoemission core level binding energy shifts

Table I: The Si-O-Si bond angle, Si-O bond distance, and number of tetrahedrons per ring (n) for various polymorphs of SiO_2.

	Si-O-Si BOND ANGLE	Si-O BOND DISTANCE	n
Quartz			
Low temperature	144 °	2.60-2.67 Å	6
High temperature	144	2.60	6
coesite	120	2.60-2.67	4
tridymite (high T)	140-173	2.63	
cristobalite (high T)	142-180	2.63	
ß-crystobalite	> 165		7,8,9
keatite	154		5,7,8

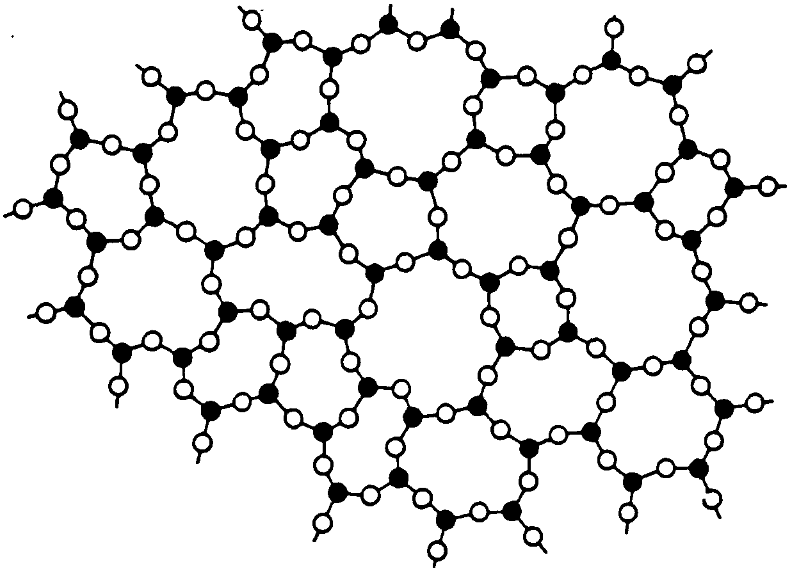

Figure 8: Schematic of the ring network in a hypothetical A_2O_3 glass network (from Zachariasen, W. H., J. Am. Chem. Soc., 54, 3841 (1932). In this hypothetical oxide network, pyramids are linked via bridging oxygen atoms. In SiO_2, SiO_4 tetrahedrons are linked via bridging oxygen atoms.

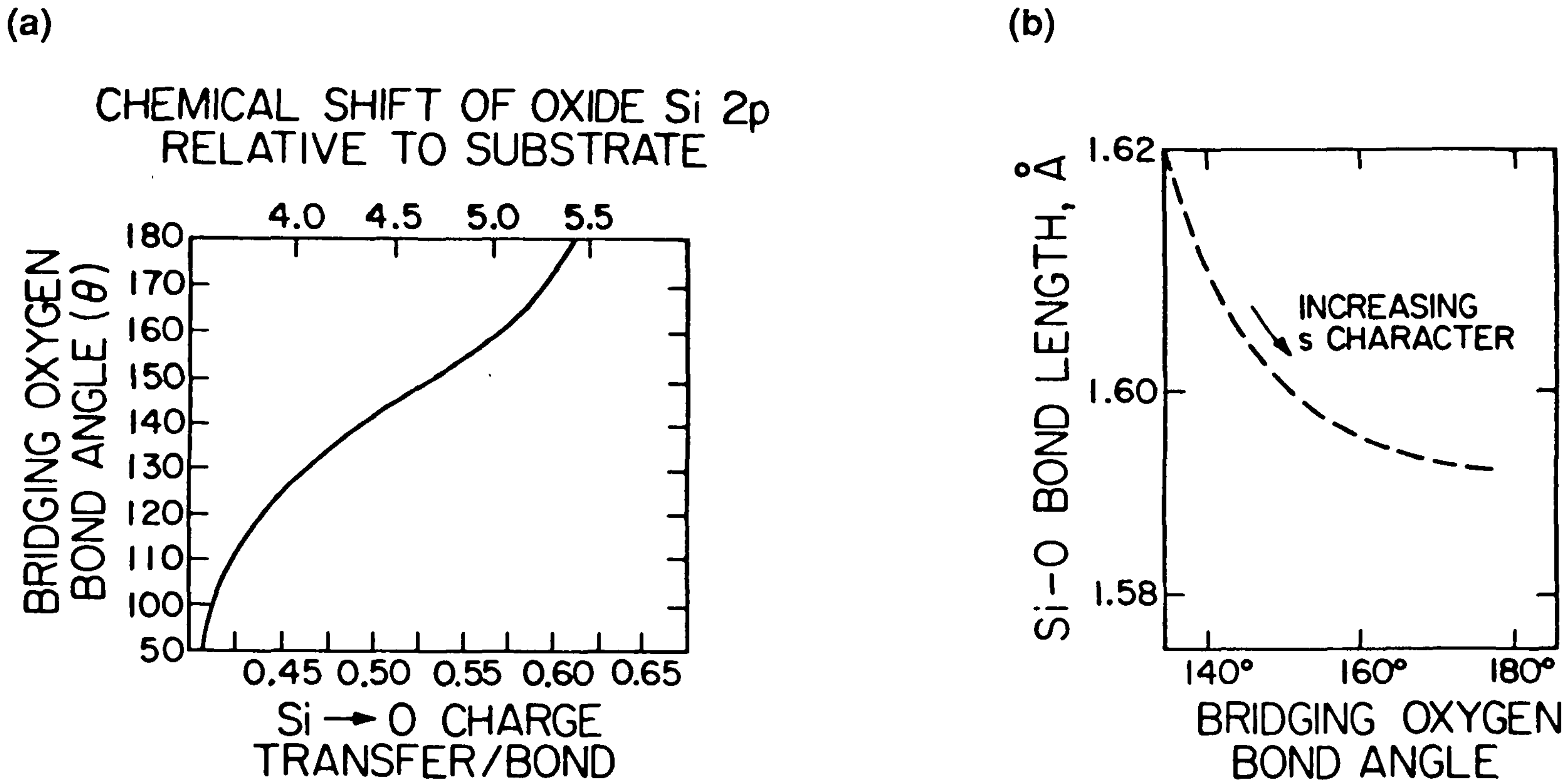

Figure 9: (a) The silicon-to-oxygen fractional charge transfer per bond as a function of the Si-O-Si bridging bond angle. Also shown is the conversion of charge transferred to the chemical shift between the Si 2p substrate and oxide signals. (See reference 6). (b) Experimental bond length versus bond angle for coesite (adapted from G. V. Gibbs, E. P. Meagher, M. D. Newton, and D. K. Swanson, in *Structure and Bonding in Crystals I*, M. O'Keefe and A. Navrotsky, Eds., (Academic Press, New York, 1981), p. 195).

and such complex phenomena as charge transfer, rehybridization, and bond length changes is not possible at this time. However, the general trend expressed in figure 9a remains correct. The smaller the Si-O-Si bond angle, the lower the binding energy of the Si core levels. We therefore interpret the shift towards lower binding energy with decreasing oxide thickness shown in figure 4 as being the result of a shift in the distribution of Si-O-Si bond angles towards angles smaller than those found in bulk SiO_2. Bulk amorphous SiO_2 can be expected to have an angle distribution centered around 144°, which is the angle found in α-quartz and represents the most stable and unstrained of the possible angles. Therefore, in the near-interfacial SiO_2, the distribution of Si-O-Si bond angles has shifted towards a value significantly less than 144°. Our earlier calculations suggest that the near-interfacial bridging bond angles are distributed around 120°.

This shift in bond angles has significant implications regarding the network structure of the near-interfacial SiO_2. By examination of figure 8, one can see that larger bridging bond angles will result in a ring network with relatively large rings of 6 to 8 tetrahedrons per ring (α-quartz consists of ordered rings with 6 tetrahedrons per ring). The smaller the bridging bond angle, the fewer the number of tetrahedrons that may be linked within a ring. We suggest, therefore, that SiO_2 near the SiO_2/Si interface is structurally distinct from bulk SiO_2 in that the SiO_2 interconnecting ring network consists of significantly smaller rings (as small as 4-5 tetrahedrons/ring, based on early calculations) than those found in bulk SiO_2 (6-8 tetrahedrons/ring).

The decrease in the average network ring size in the near-interfacial region is a natural consequence of the "lattice-mismatch" between SiO_2 and crystalline Si. The larger Si-O bond length in SiO_2 as compared to the Si-Si bond length in Si requires that the Si-O-Si angle decrease if the SiO_2 network is to bond to the Si crystal surface with a high level of perfection. The SiO_2/Si interface is known, in fact, to be relatively perfect since less than 5 $\times 10^{10}$ interface states/cm^2 are typically obtained in device-quality gate oxides. It is reasonable to suggest that the large "lattice-mismatch" between SiO_2 and Si is accommodated by the flexible Si-O-Si bond angle in the near-interfacial region of the SiO_2, permitting near-perfect bonding of the oxide network to the Si substrate with few dangling orbitals or other interface states.

III.A.2. Analysis of Core Level Intensities

The intensities of the Si 2p core level oxide and substrate signals also provide evidence for a structurally distinct region of SiO_2 near the SiO_2/Si interface. The ratio of the core level oxide signal intensity to the substrate signal intensity depends upon such parameters as: (1) the oxide thickness, (2) the atomic density of Si in the oxide and in the substrate, (3) the electron mean free path in the oxide and in the substrate, and (4) a variety of spectrometer factors not important for the discussion here. Given only the experimentally determined oxide/substrate intensity ratios for different oxide thicknesses, one may calculate the product of the electron mean free path, λ, and the atomic density of Si in the oxide, D, as a function of thickness.[7] This product will hereafter be denoted as the $D\lambda$ product. $D\lambda$ may be used as a "structural parameter" to monitor any structural changes in the oxide that affect either the atomic density or mean free path of electrons within the oxide. It is determined relative to the $D\lambda$ product of the substrate by normalizing the oxide/substrate ratios found at different oxide thicknesses with the absolute intensity of the Si 2p signal from a clean Si substrate. It is important to note that this procedure results in an average $D\lambda$ value for each layer of oxide removed during a chemical profile as schematically shown in figure 10a. The details of this

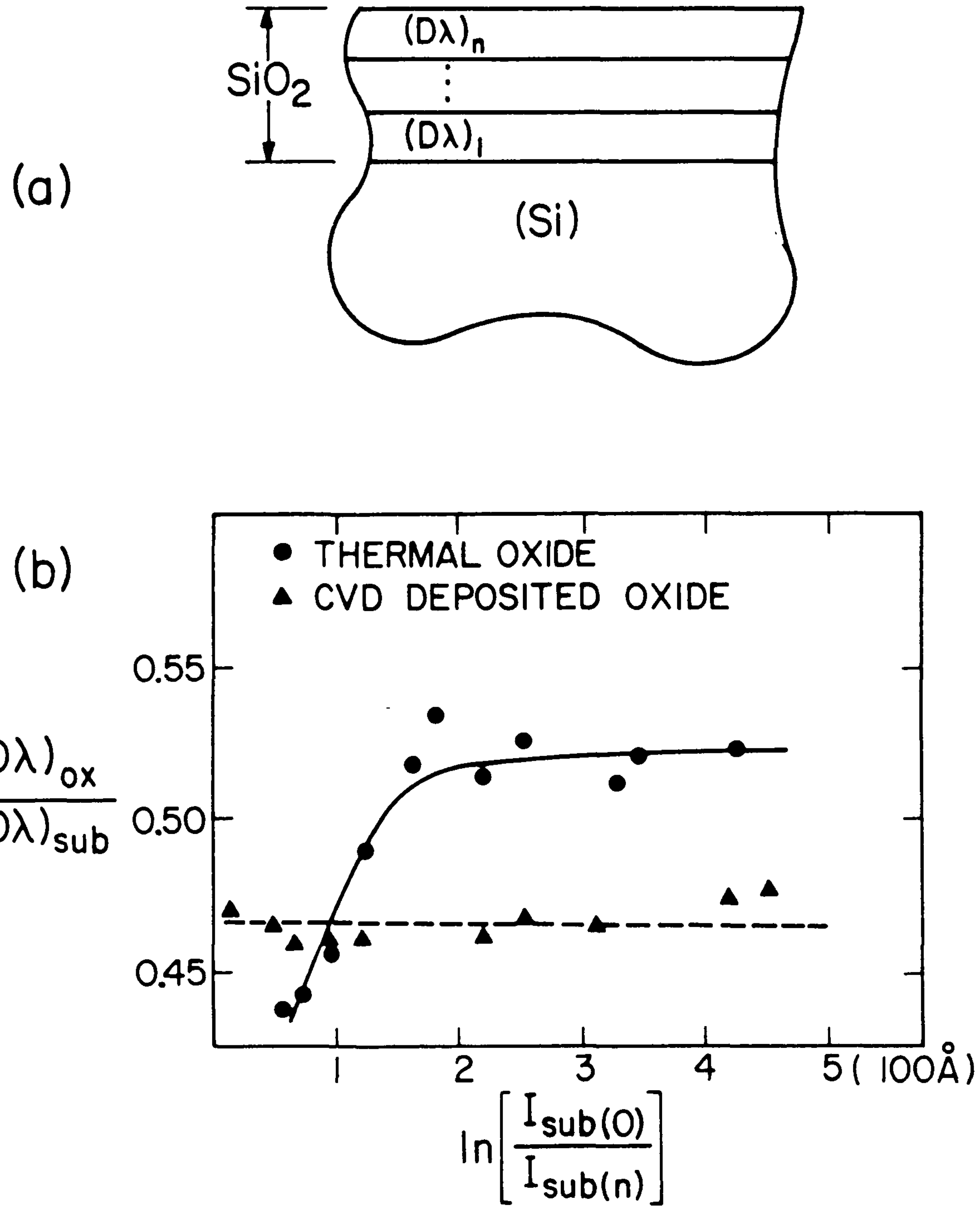

Figure 10: (a) Schematic illustrating the layer approximation used in the Dλ calculation. The material removed during a given etch step corresponds to a layer. (b) A Dλ profile for a thermal oxide on Si (100) and a deposited CVD oxide.

procedure may be found in reference 7. The Dλ product as a function of oxide thickness for a typical thermal oxide is shown in figure 10b. For oxide thickness greater than 30-50 Å, the Dλ product is essentially constant. Below 30-50 Å, the Dλ product decreases rapidly. This is the same oxide thickness regime over which the oxide Si 2p core level signal is observed to shift towards lower binding energy, as discussed in section III.A.1. The rapid decrease in the Dλ product in the near-interfacial region reflects a structural change in the SiO_2 that affects either the Si atom density in the oxide and/or the electron mean free path. A decrease in the average number of SiO_4 tetrahedrons per ring in the network structure of the SiO_2 in the near-interfacial region, a conclusion discussed in the previous section, is consistent with such a change in the Dλ product since the atomic density of Si in the oxide is directly related to the network ring size.

For comparison, also plotted in figure 10b is a Dλ profile of a CVD oxide deposited onto silicon. A deposited oxide is not forced to "lattice match" at the interface to the same degree as a thermal oxide and, as a consequence, one would expect the Dλ product for a deposited oxide to show less variation with thickness near the interface. As shown in figure 10b, we find the Dλ product for a CVD oxide to be constant throughout the film. This supports our suggestion that the decrease in the average ring size in the oxide network in the near-interfacial region is due to the "lattice-mismatch" between amorphous SiO_2 and crystalline Si.

The Dλ profiles discussed above require that the oxide be chemically thinned using the spin-etch approach discussed in section II.C. One must question whether the physical removal of oxide modifies the underlying oxide structure. This could occur because of impurity (hydrogen) incorporation during profiling and /or a relaxation of the ring network in the near-interfacial region after the constraining overlayer of bulk SiO_2 had been removed. To address this issue, we have used the Stanford Synchrotron Radiation Laboratory (SSRL) facilities for variable photon energy photoemission studies of thin thermal SiO_2 films on Si.[8] Variable incident photon energy permits one to vary the kinetic energy of the photoejected electron and, hence, its mean free path. As schematically diagrammed in figure 11, this permits "profiling" the oxide structure without physically thinning the SiO_2 beyond 50 - 100 Å. A $D\lambda$ profile similar to that already discussed above may then be calculated.

Figure 12 displays Si 1s spectra obtained from a 53 Å oxide in the photon energy range of 1950 - 3700 eV, corresponding to an electron mean free path range of 10 - 50 Å. Notice the change in the relative intensity of the SiO_2 (1841.5 eV) and Si (1836.5 eV) derived peaks as the incident photon energy is varied. At a photon energy of 1950 eV, only the SiO_2 component is observed, while at 3700 eV, the SiO_2 and Si peaks are of equal intensity. The absolute intensities of the Si 1s spectra are decreasing with increasing photon energy because of a decrease in the photoelectron cross section.

Recall from figure 4 that as the SiO_2 is physically removed and examined with fixed photon energy photoemission, the SiO_2 signal begins to shift towards lower binding energy begining at 30-50 Å of oxide. We attributed this shift to a region of structurally distinct SiO_2 which had been exposed by the chemical etch. If this structurally distinct region is indeed unrelated to a change in the oxide structure caused by the etch itself, it should be observable in the variable photon energy experiments as well. The binding energy shift, however, should be considerably weaker since the variable photon energy experiments yield a signal which represents a weighted average over the oxide in which the near-interfacial component is still far smaller than the oxide component near the vacuum/oxide surface. Figure 13 plots the separation of the centroids of the SiO_2 and Si signals

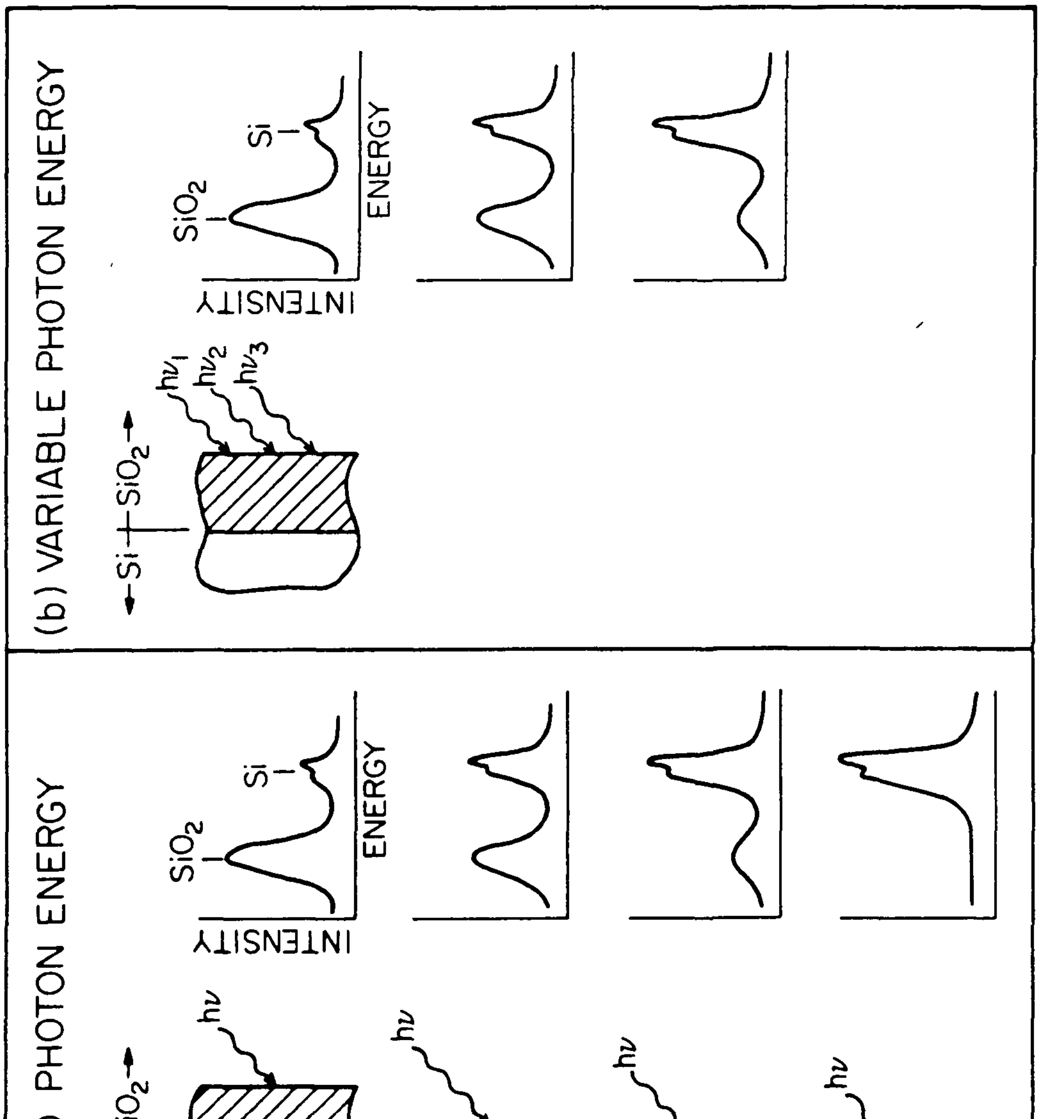

Figure 11: Schematic illustration of "profiles" obtained using (a) fixed photon energy photoemission in conjunction with chemical profiling techniques and (b) variable photon energy photoemission.

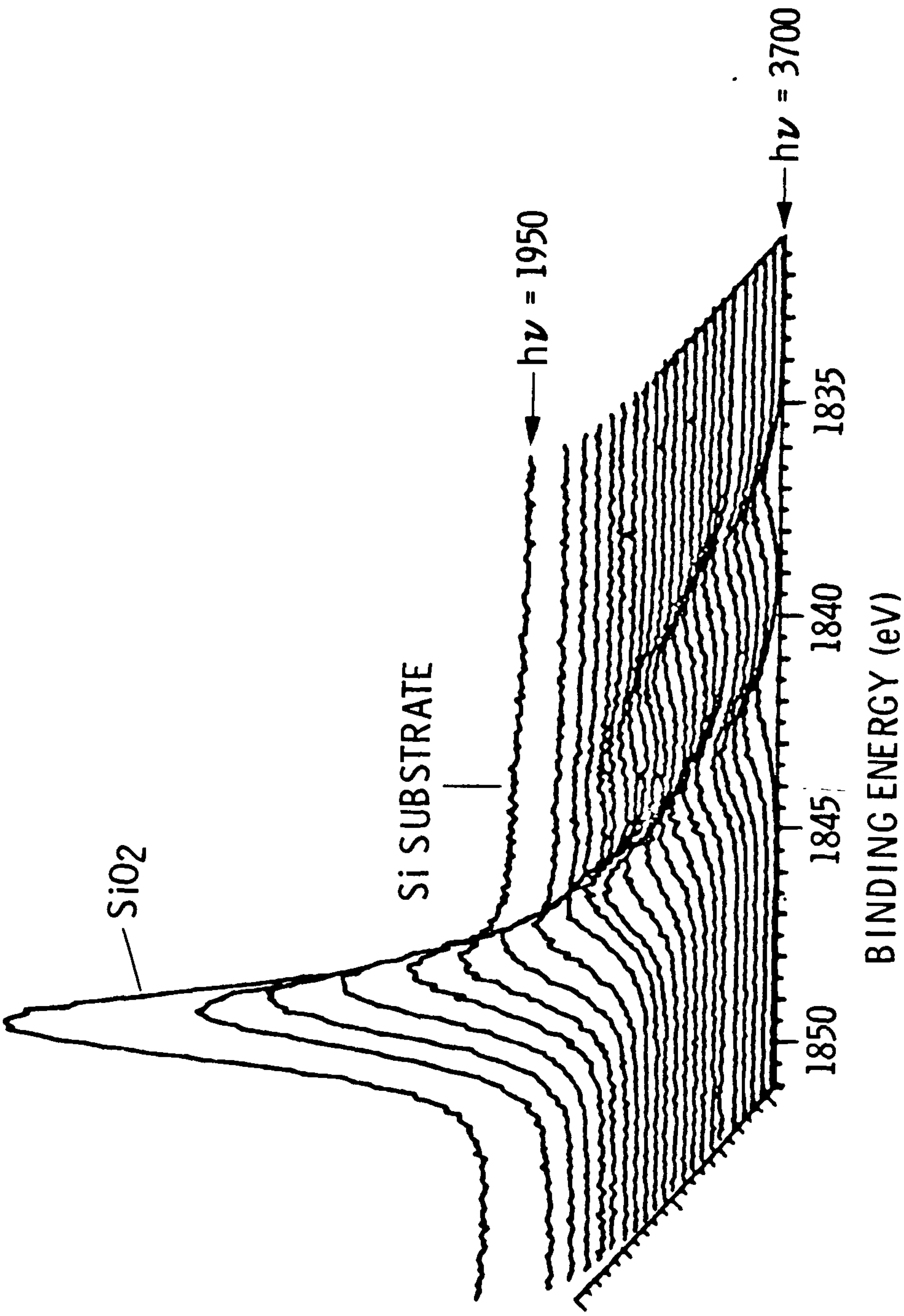

Figure 12: Si 1s spectra from a 53 Å thermal oxide taken at photon energies 1950 (top), 2000, 2050, 2100, and every 100 to 3700 eV. The drop in intensity is a cross-section effect. At 3700 eV (bottom) the substrate and oxide peaks are of comparable intensity.

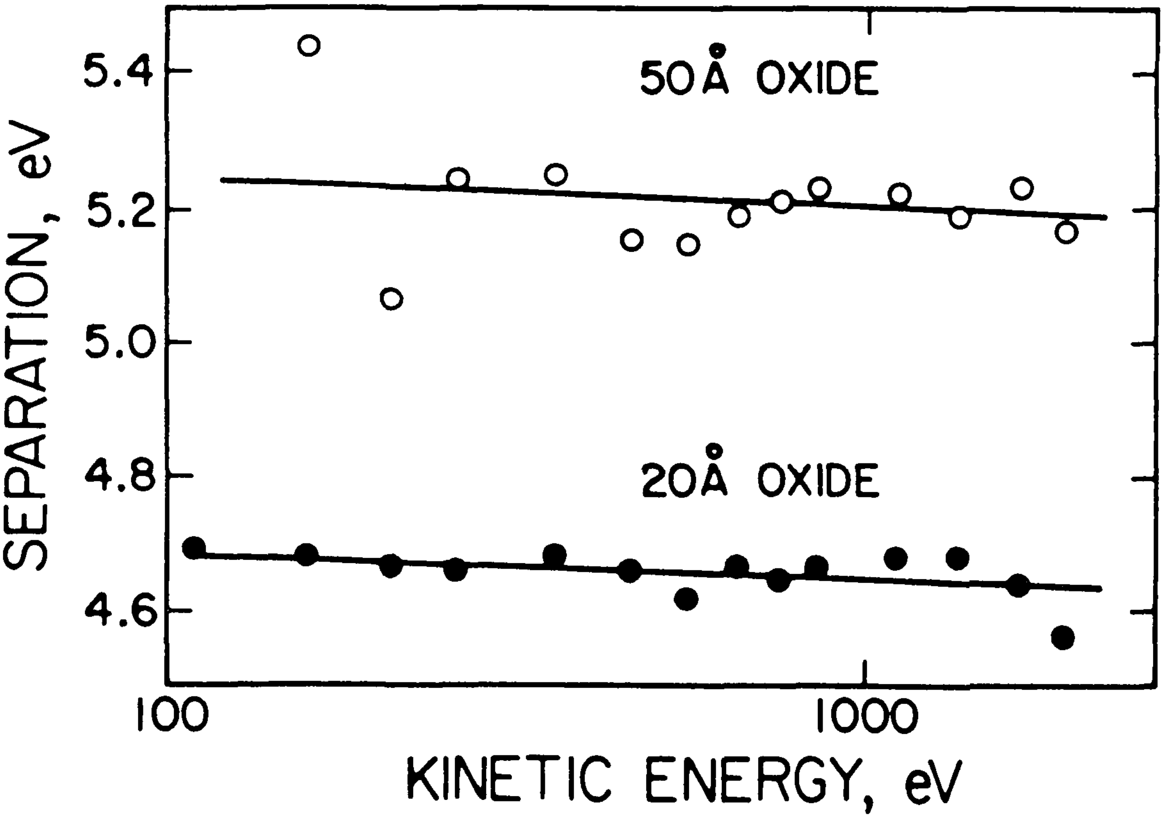

Figure 13: Substrate-oxide Si 1s peak separation as a function of electron kinetic energy. The separation is determined by a centroid method. The sloping line is intended as a guide to the eye, and does not represent a fit to the data points.

as a function of the electron kinetic energy for 50 Å and 20 Å oxides. Although the relative shift is small compared to that observed in figure 4, as was anticipated, the downward slope of the data clearly indicates that the peak shift as a function of oxide thickness is not merely a result of the oxide thinning.

A Dλ product can be calculated from the synchrotron radiation photoemission spectra presented in figure 12 which is similar to that already discussed in figure 10b for fixed photon energy photoemission. The results of this calculation are shown in figure 14, the details of which may be found in reference 8. There is one important difference in the Dλ products obtained by these two experimental approaches, other than the fact that one requires physically thinning the oxide while the other does not. The Dλ product in figure 10b represents the average Dλ value for each individual layer removed during the chemical etch. The Dλ value in figure 14 is the average value of Dλ over the entire observation depth of the spectroscopy. As the electron kinetic energy is increased, the electron mean free path is increased, and, hence, more of the near-interfacial region is included in the weighted Dλ average. As can be seen in figure 14, as the observation depth in the oxide increases (increasing kinetic energy), the average Dλ value decreases. The dotted line represents the variation of Dλ expected for bulk SiO_2 simply because of the kinetic energy dependence of λ. Clearly, the decrease in Dλ with increasing kinetic energy for a 53 Å oxide is greater than that indicated by the bulk curve. This corroborates the results obtained using fixed photon energy photoemission indicating that there exists a near-interfacial region with a lower Dλ product than that of bulk SiO_2. It furthermore demonstrates that such a region is not due to the chemical profiling procedure.

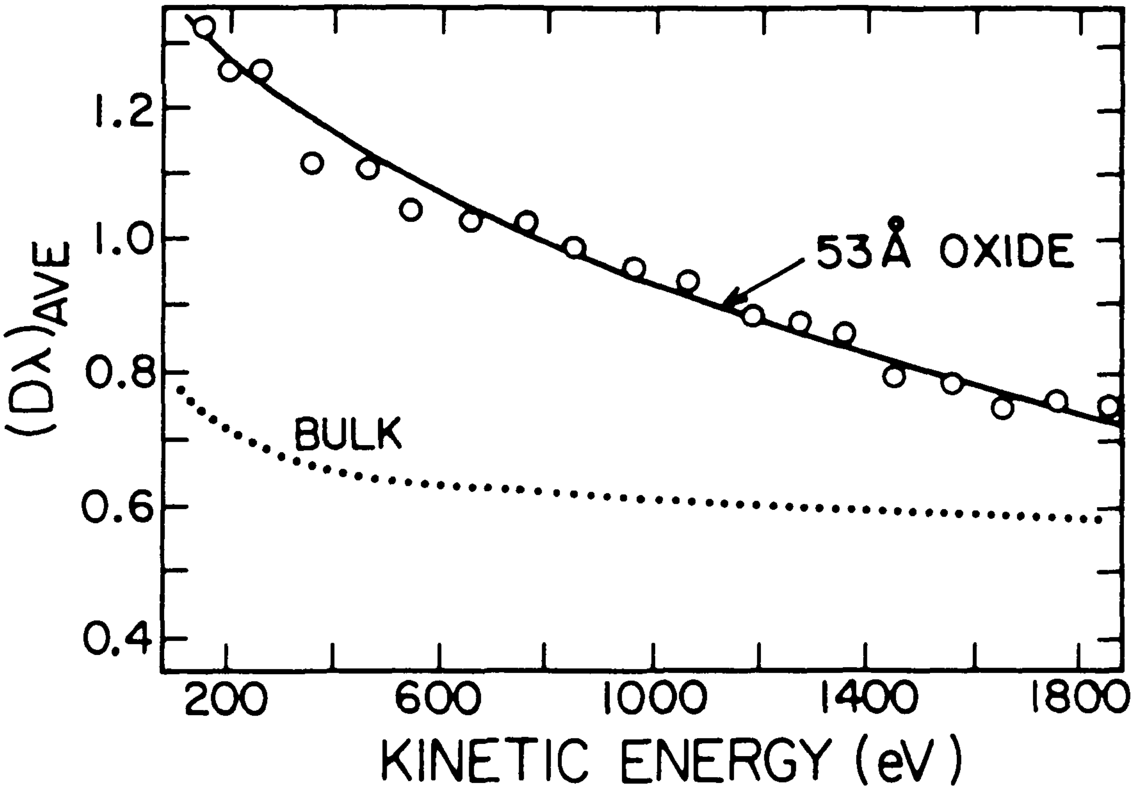

Figure 14: The average Dλ product versus kinetic energy for a thermal oxide on Si (100). The dotted curve marked "bulk" represents the bulk value of Dλ and reflects the variation in Dλ due to the kinetic energy dependence of λ.

III.A.3. Chemical Etch Rates

The dissolution of SiO_2 by hydrofluoric acid is sensitive to the structure of the interconnecting ring network. For example, α-quartz will dissolve more slowly in HF than amorphous SiO_2. In the chemical profiling experiments already described, controlled amounts of HF in ethanol are used to thin the oxide. By using XPS to monitor the oxide thickness for a given HF exposure, the dissolution rate of the oxide can be determined as a function of the oxide thickness. The reaction rates for two different oxide processing conditions are shown in figure 15. There is little variation observed in the reaction rate as the oxides are etched from 800 Å to 100 Å. Below 100 Å, the oxide that did not receive a post-oxidation anneal shows a decrease in etch rate while the oxide receiving an anneal shows a significant increase in etch rate. This illustrates that not only is there a structural difference in the oxide in the near-interfacial region of the SiO_2, but that this structural difference is sensitive to the processing conditions.

III.A.4. SEXAFS

Surface extended X-ray absorption fine structure (SEXAFS) measurements were obtained directly indicating the shortening of the Si-Si second nearest neighbor distance in the near-interfacial region of SiO_2 on Si.[9] In these experiments, the Si and SiO_2 KLL Auger line intensities were measured as a function of photon energy from the Si 1s threshold of 1840 eV to 2500 eV. Data were obtained on 20 Å and 750 Å oxides. If indeed the near-interfacial region of the oxide consists of a ring network structure in which the average Si-O-Si bond angle linking SiO_4 tetrahedra is reduced as compared to the bulk oxide, one would expect to see an overall shift in the distribution of Si-Si distances toward smaller values for the 20 Å oxide relative to the 750 Å oxide.

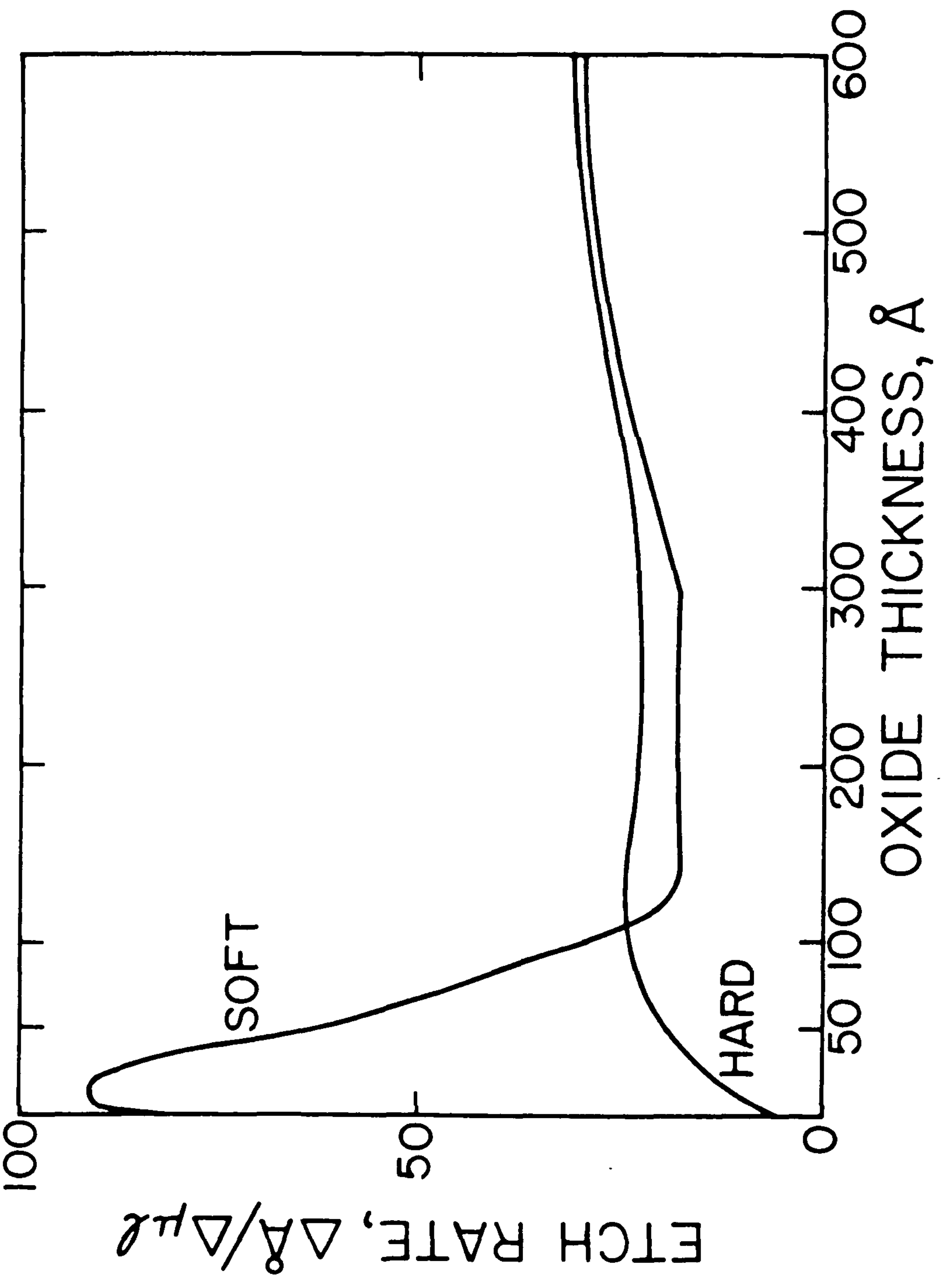

Figure 15: Plot of the oxide removal rate as a function of oxide thickness for radiation hard and soft gate oxides. The rate is expressed in relative units.

The SEXAFS spectra after a transform to momentum space and background subtraction are shown in figure 16. It is clear that the 20 Å oxide has a more complicated frequency distribution, consistent with a broader distribution of Si-O-Si bond angles. Fourier transforming the spectra in figure 16 results in the spectra shown in figure 17. The largest peak in each spectra corresponds to the Si-O bond distance which is approximately 1.6 Å (the phase factor has shifted the peaks approximately 0.5 Å in figure 17). For the 20 Å oxide, two additional peaks are observed at 1.9 Å and 2.6 Å. For the thicker oxide, a single broad peak occurs over this same region. Computer modeling shows that this unexpected structure is due to the beating pattern between closely spaced frequencies and that the shape of this pattern is extremely sensitive to the relative intensities of the components. Using a two-component model, the two-peak pattern observed for the 20 Å oxide is consistent with the presence of 120^o and 144^o Si-O-Si bond angles in the approximate ratio of 1 to 1. The broad pattern observed for the 750 Å oxide is consistent with a 120^o to 144^o component ratio of 1 to 3. These results clearly indicate the increasing proportion of smaller rings in the near-interfacial oxide region as compared to the bulk.

III.B. Comparison of Hard and Soft Gate Oxides

In section III.A above, evidence was presented for the presence of a structurally distinct region of SiO_2 near the SiO_2/Si interface. The evidence supports a picture for the oxide in which the near-interfacial region is composed of an interconnecting ring network with a distribution of ring sizes which are smaller than those present in the bulk SiO_2. In this section, data are presented which indicate that the near-interfacial oxide structure for radiation hard oxides is different in detail from that found for radiation soft oxides. Specifically, we find that not only

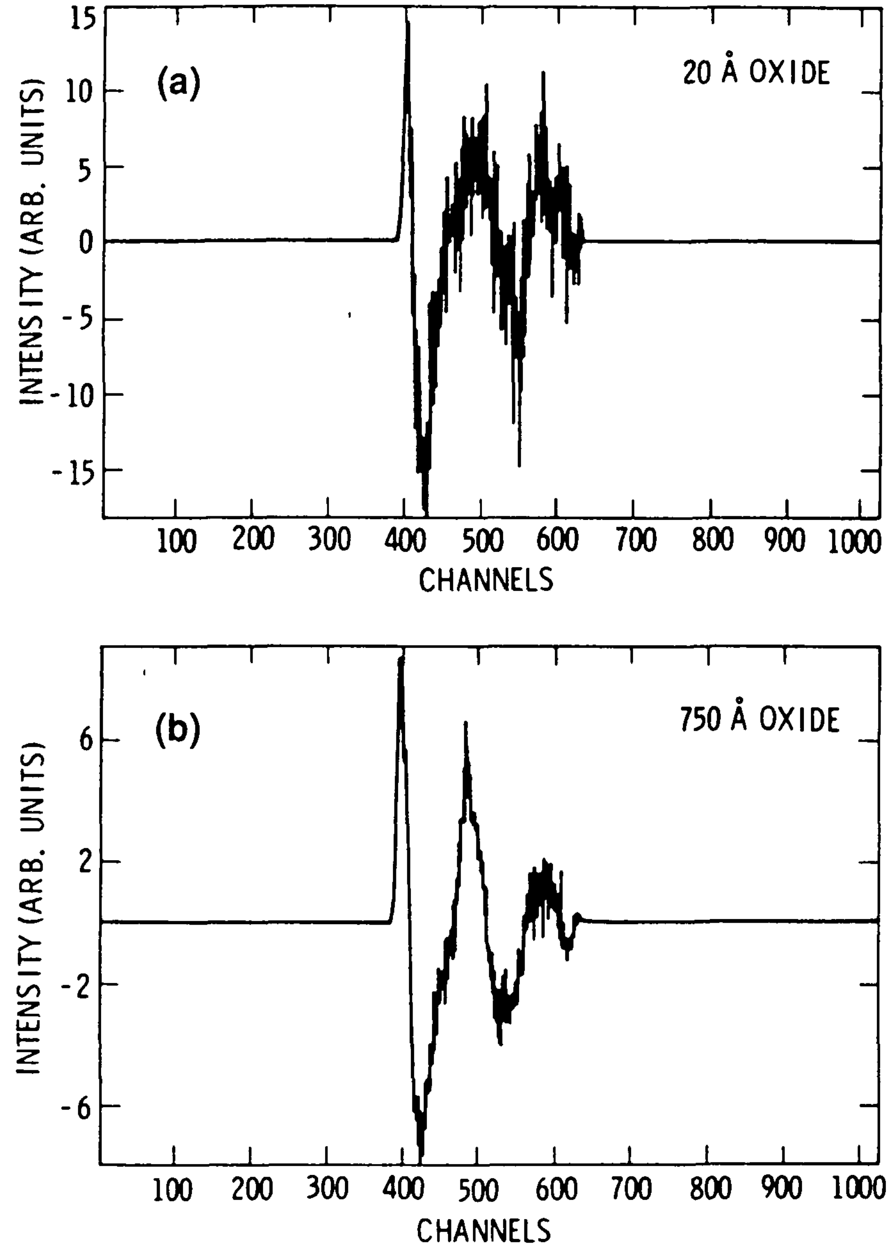

Figure 16: Surface extended X-ray absorption fine structure (SEXAFS) spectra after transform to momentum space and background subtraction. (a) KLL yield, 20 Å oxide. (b) KLL yield, thick oxide.

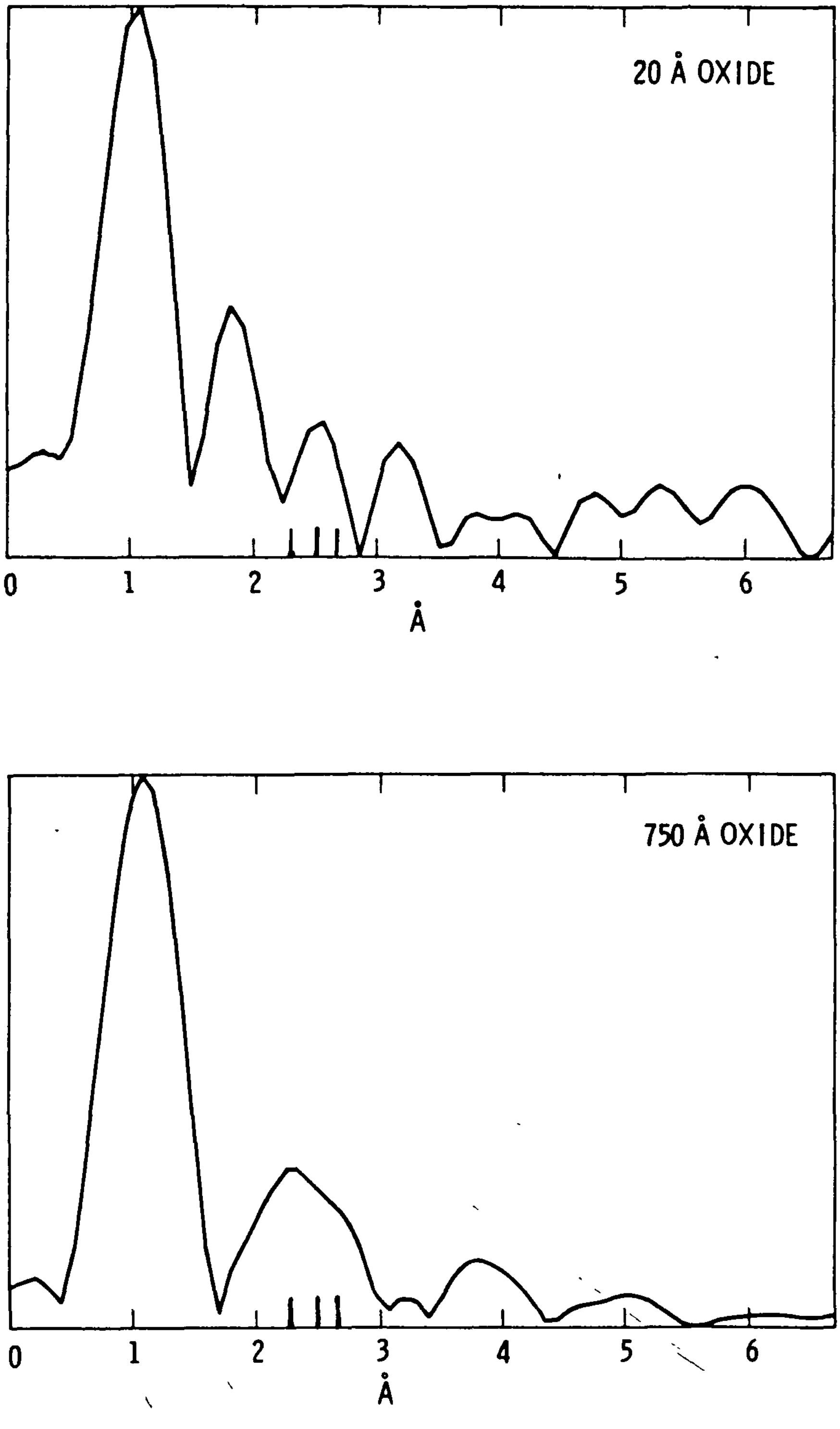

Figure 17: Fourier transform of the spectra in figure 16. Note that the peak positions do not directly indicate interatomic distances, but must be phase shifted.

is the distribution of smaller ring sizes near the SiO_2/Si interface different for hard versus soft oxides, but that the spatial extent of this structurally-distinct SiO_2 is different as well.

The structural differences in hard and soft oxides were examined using both fixed and variable photon energy photoemission. Core level binding energy analysis, as discussed in section III.A.1, was not found to be sufficiently sensitive to the structural differences in oxides processed under different conditions. The shift of the Si 2p oxide peak toward lower binding energy for oxides less than 30-50 Å thick is accompanied by changes in lineshape which are difficult to quantify without the use of complex mathematical analysis such as maximum entropy deconvolution. In contrast, the core level intensity analysis, as discussed in section III.A.2, is relatively simple to execute and is quite sensitive to subtle changes in the oxide network structure.

The $D\lambda$ product obtained from an analysis of core level intensities has been discussed in section III.A.2 and the reader should refer to this section for details of this calculation. Recall that the variations in the $D\lambda$ product reflect any structural changes in the oxide that alter the density of Si atoms and/or the electron mean free path in the oxide. Absolute values of D or λ need not be assumed since we are interested in relative changes within the oxide.

A plot of the $D\lambda$ product as a function of oxide thickness for hard and soft pyrogenic oxides is given in figure 18. The $D\lambda$ product is essentially constant for both hard and soft oxides for oxide thicknesses greater than 30-50 Å. Notice, however, that the magnitude of the $D\lambda$ product is largest for the hard oxide. In general, we observe that the magnitude of $D\lambda$ for thicknesses greater than 30-50 Å varies from oxide to oxide, depending upon the details of the oxide processing conditions. Indeed, there are conditions under which the magnitude of $D\lambda$ for a

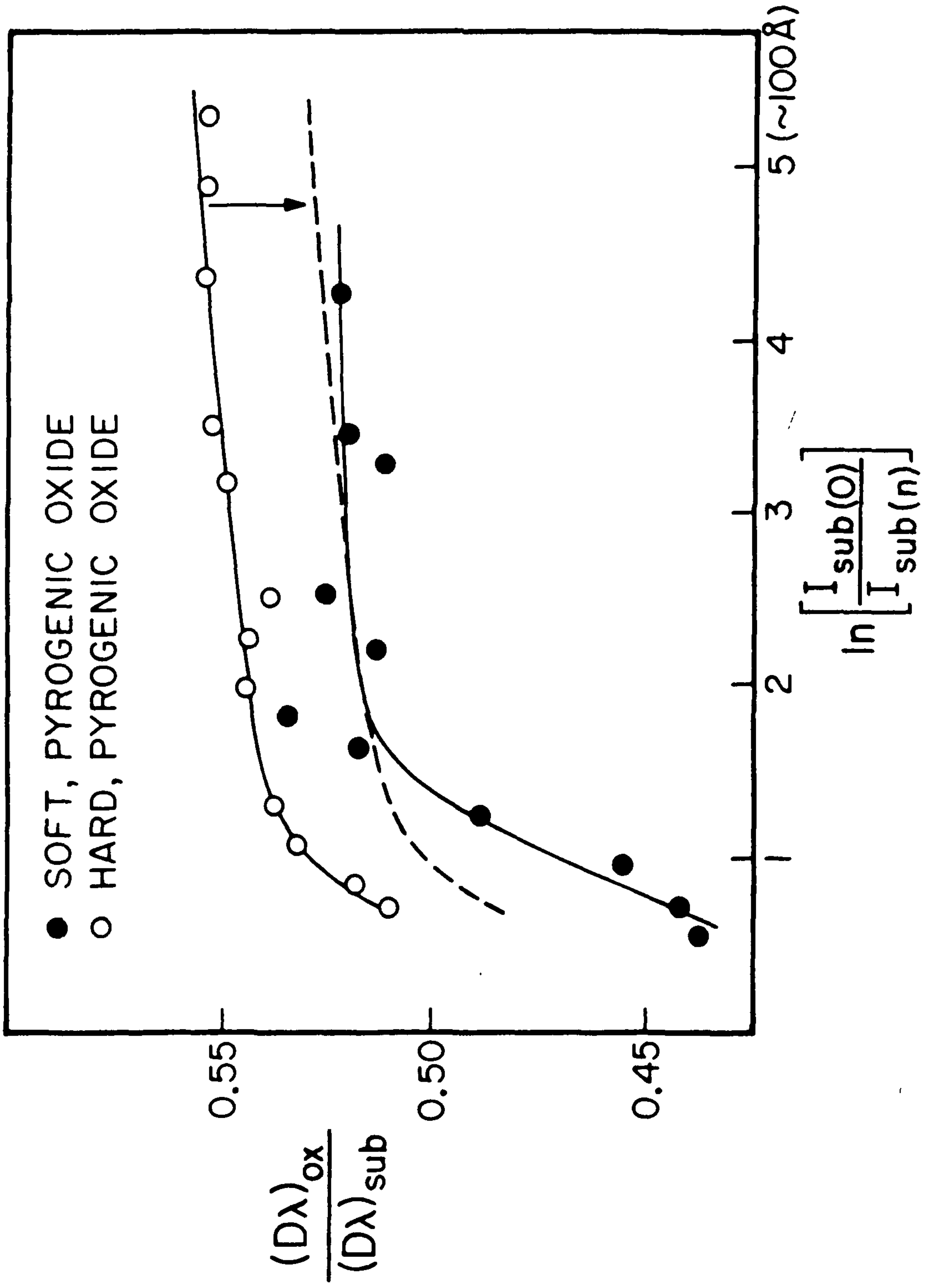

Figure 18: Plot of the Dλ product as a function of oxide thickness for radiation hard and soft pyrogenic gate oxides.

hard oxide has been less than that observed for the corresponding soft oxide. These results indicate that although within a given oxide the bulk structure is essentially invariant, there are structural differences from oxide to oxide. We have not attempted to characterize these structural differences in the bulk of the oxide during the effort being reported here.

Ignoring bulk structural differences for the moment, one can align the bulk (greater than 30-50 Å oxide) Dλ values for hard and soft oxides by shifting the curve for the hard oxide such that it overlaps the curve for the soft oxide (see the dashed line in figure 18). Comparing the dashed curve for the hard oxide with the curve for the soft oxide, it is clear that Dλ for the soft oxide begins to decrease signficantly before the hard oxide. This indicates that the spatial extent of the structurally-distinct SiO_2 is larger for the soft as compared to the hard oxide. This trend is independent of the relative magnitudes of the Dλ curves. Estimation of the precise spatial extent of the near-interfacial region for the two types of oxides is difficult since it requires knowledge of the absolute values of D and λ.

Variable photon energy photoemission experiments were also performed on hard and soft oxides at the Stanford Synchrotron Radiation Laboratory. As discussed in detail in section III.A.2, such experiments permit one to "profile" an oxide by varying the kinetic energy of the photoejected electron. In this way, an average (albeit weighted toward the surface) Dλ may be obtained over the probe depth of the spectroscopy. The larger the kinetic energy of the electrons, the deeper the probe depth. Figure 19 shows the Dλ curves obtained for an 18 Å soft oxide as well as 53 Å and 11 Å hard oxides. These oxides were prepared from thick oxides using the chemical etching procedure described in section II.C. Several observations can be made from the data in figure 19. First, for all three oxides, the average Dλ value decreases as the probe depth increases. As

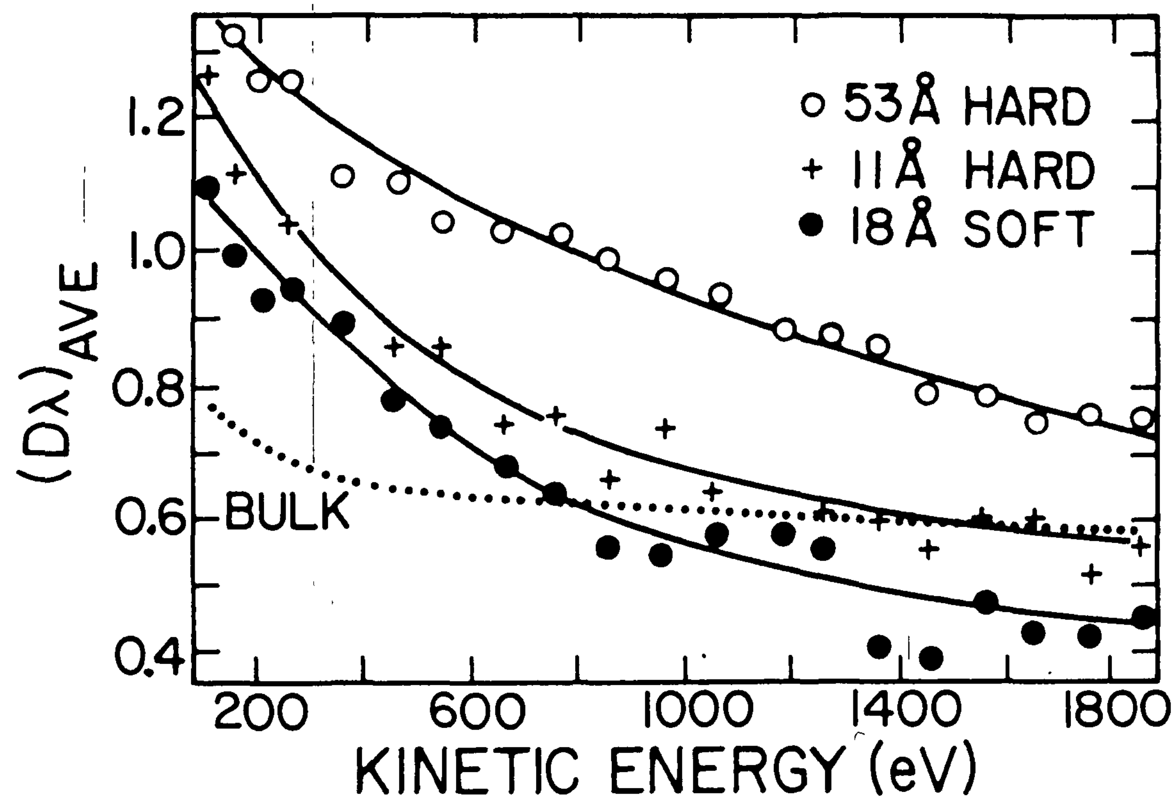

Figure 19: Plot of the average Dλ product versus kinetic energy for an 18 Å radiation soft oxide and for 11 Å and 53 Å radiation hard oxides. These oxides were initially thick gate oxides subsequently thinned using the chemical techniques described in section II.

discussed in section III.A.2, this indicates that $D\lambda$ is indeed smaller in the near-interfacial region as compared to the bulk region and that its decrease is not an artifact of the chemical etching. That the $D\lambda$ curve for the 11 Å hard oxide is below that for the 53 Å hard oxide is further demonstration that $D\lambda$ is decreasing toward the interface. Second, the $D\lambda$ curve for the 18 Å soft oxide falls below that of the thinner 11 Å hard oxide. This is consistent with the fixed photon energy experiments in which it was concluded that the spatial extent of the near-interfacial SiO_2 is largest for soft oxides.

IV. *IN-SITU* ELECTRON STRESS EXPERIMENTS

IV.A. Introduction

This section summarizes results from *in-situ* electron irradiation experiments devised to examine the effect of ionizing radiation on the network structure of SiO_2 on Si.[10,11] The XPS spectrometer is equipped with a low-energy electron gun capable of irradiating the sample with electrons of kinetic energy from 0 to 10 eV. The maximum current density to the sample during these experiments was approximately 10^{-5} amps per square cm. Irradiation experiments were performed varying the oxide thickness and sample temperature using thin thermal oxides grown at JPL and thick gate-oxide films provided by Sandia. The thin (6 to 86 Å) oxides produced at JPL were grown in dry oxygen at 850° C on n-type (100) Si wafers. The Sandia samples have been described in section II.A.

The experiment entails irradiating a SiO_2/Si sample with electrons under UHV conditions while simultaneously recording XPS core level spectra. Initial spectra were obtained before irradiating the sample with electrons. The sample was then irradiated with 10 eV electrons for 10 -11 hours in an effort to maximize the damage produced. These energetic electrons create holes in the silicon substrate and oxide via impact ionization. The strong negative surface potential on the oxide produced by the electron irradiation injects energetic holes from the substrate into the interfacial region of the SiO_2. By simultaneously monitoring the Si 2p core level during and after electron irradiation, one can determine whether any chemical modifications are being induced in the SiO_2 network.

During the actual irradiation, the Si 2p spectra are significantly broadened and shifted by charging effects and little information can be extracted from the data. This has been discussed previously and is illustrated in figure 5, which shows the Si 2p spectra obtained during irradiation with electrons of increasing kinetic energy. Notice that as the negative bias increases the observed energy shift of the SiO_2 peak relative to the Si substrate peak decreases and the width of the SiO_2 manifold increases. After the electron source is turned off, however, the negative surface charge quickly tunnels away, removing the strong voltaic shifts and broadening of the SiO_2 signal. The SiO_2 peak shifts back to its original binding energy position, but an additional feature not present in the unirradiated spectra appears. This additional feature lies approximately 2.3 eV higher in binding energy than the substrate signal and decays slowly with time until only a small residual signal remains, as shown in figure 20. The damage feature occurs at a binding energy consistent with a Si^{+3} chemical state (the Si atoms in SiO_2 and Si are in Si^{+4} and Si^0 states, respectively) and this feature will hereafter be referred to as a Si^{+3} state. Note that as the intensity of the Si^{+3} state slowly decays in figure 20, the intensity of the SiO_2 manifold increases.

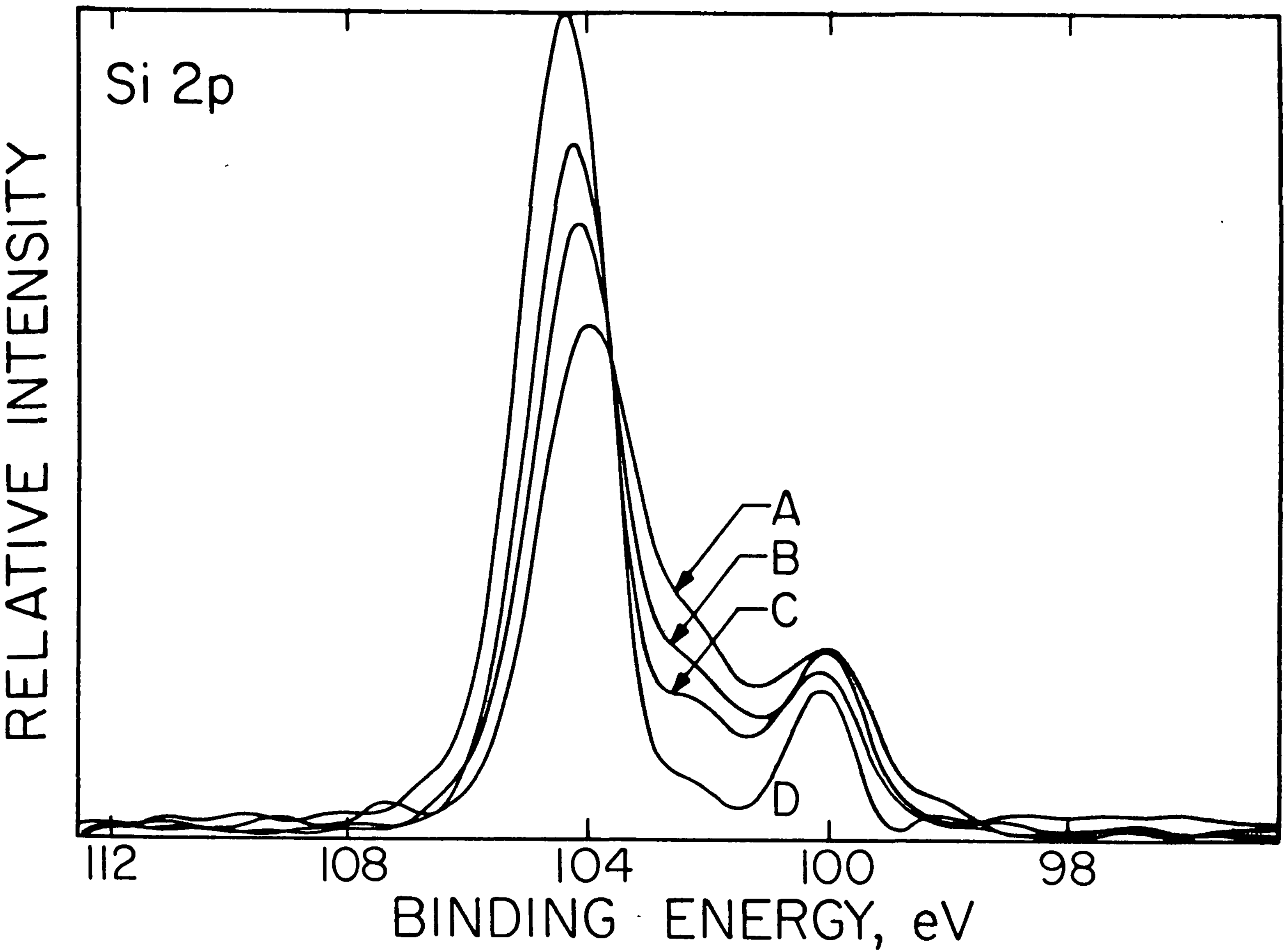

Figure 20: Plot of the sequential decay of Si 2p spectra (A to D) for a nominally radiation hard gate oxide after 10 eV electron irradiation under UHV conditions.

IV.B. Oxide Thickness and Temperature Dependence

Examination of the Si^{+3} peak as a function of oxide thickness and sample temperature during irradiation provides some insight into the origin of the damage signal. No Si^{+3} species can be detected in experiments using oxides less than 28 Å in thickness. The absolute radiation-induced Si^{+3} peak intensity increases in going from a 32 Å oxide to a 41 Å oxide, then remains essentially constant up to 49 Å of oxide, and finally decreases in intensity from 52 Å to 86 Å of oxide (86 Å was the thickest oxide examined). We conclude therefore that the Si^{+3} species is being produced within the structurally-distinct near-interfacial SiO_2 region previously discussed in section III.

The temperature dependence of Si^{+3} formation was investigated using 25 Å, 48 Å, and 86 Å oxides. As before, no Si^{+3} signal could be observed for the 25 Å sample over the temperature range of 150-523 K. For the 48 Å and 86 Å oxides, as the temperature was decreased, the final intensity of the Si^{+3} signal increased. In addition, the rate of the slow decay of the Si^{+3} signal increased with increasing temperature. These experiments suggest that motion of the SiO_2 lattice is somehow involved in the production and annealing of the Si^{+3} species.

IV.C. Model for Radiation-Induced Bond Cleavage

We have proposed a model for the production of the Si^{+3} peak which involves the radiation-induced cleavage of a Si-O covalent bond within the SiO_2 network.[11,12] This model is summarized in figure 21. Recall from section III, we have presented considerable evidence that the near-interfacial region of SiO_2 on Si consists of a SiO_4 ring network with significantly smaller rings than those found in the bulk of the oxide. The smaller Si-O-Si bridging bond angles within this region are considerably strained relative to the bond angles energetically

STEP I RADIATION-INDUCED CLEAVAGE OF COVALENT BOND

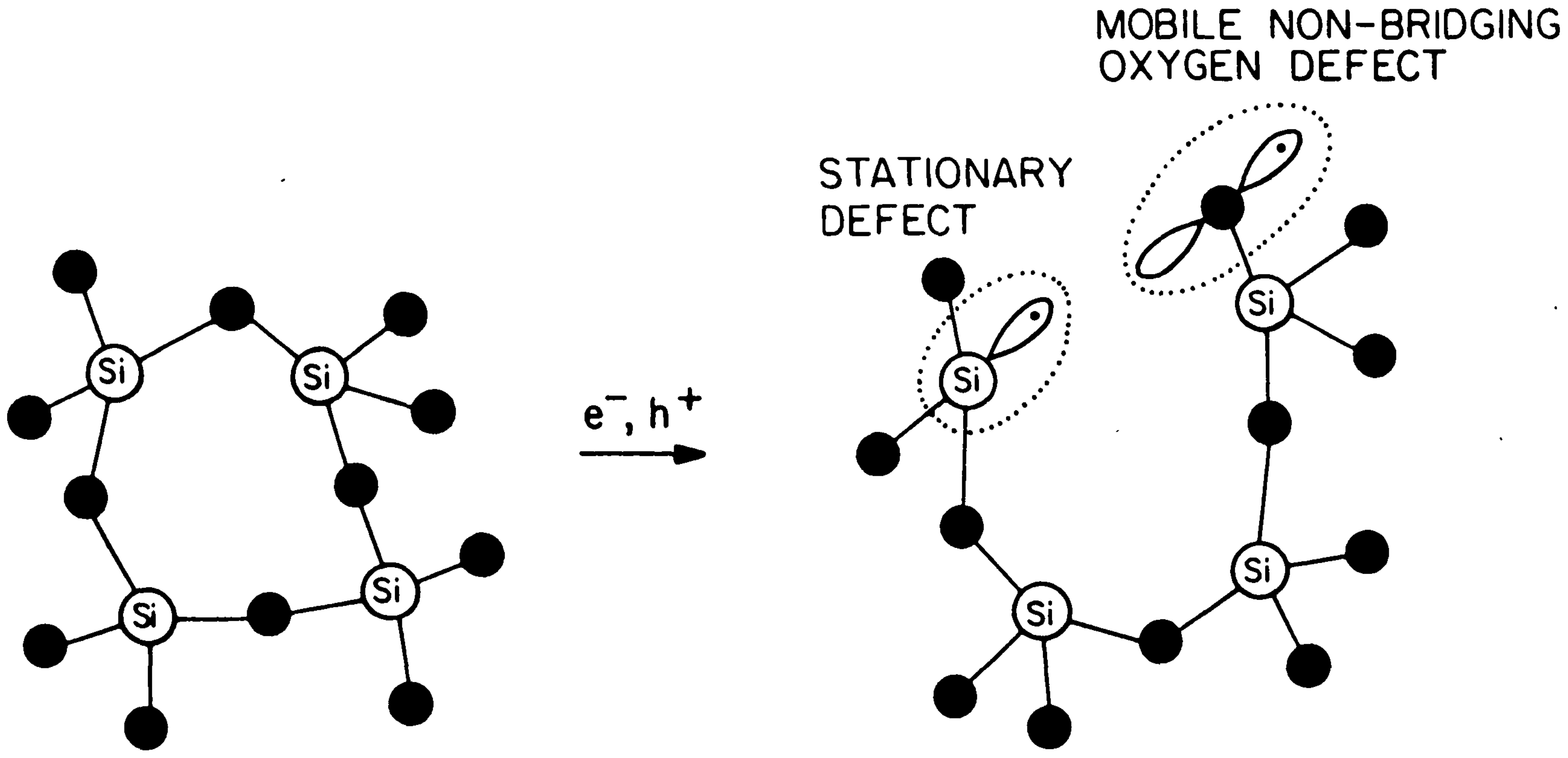

Figure 21: Illustration of the radiation-induced cleavage of a strained Si-O covalent bond in the SiO_2 network.

preferred. The capture of a hole at a strained Si-O bond in this region reduces the bond strength at this site and the strain energy can be relieved by the energetically favored rupturing of this weakened bond. The result of the cleavage of this Si-O bond is a Si^{+3} species (a Si atom bonded to three of the network oxygen atoms and having a singly occupied dangling orbital) and a Si^{+4} species (a Si atom coordinated to three network oxygen atoms and one nonbridging oxygen atom) as shown in figure 21. The Si^{+3} species is observable in the XPS data as indicated in figure 20, while the Si^{+4} species overlaps with the Si^{+4} signal of the SiO_2. The resulting species should be neutral because of the ready availability of electrons and holes in the oxide during the experiment for annihilation of any residual charge. Local relaxation of the strained SiO_2 lattice prevents the Si-O bond from simply reforming. Some site recombination can occur, as observed in the slow decay of the Si^{+3} signal in the XPS data. We suggest this is due to random electron/hole recombination, phonons, or some other phenomenon permitting the broken bond species to come sufficiently close to reform the bond. We suggest that the cleavage of the Si-O bonds occurs primarily in the near-interfacial region of the SiO_2 because in the bulk SiO_2 region the network structure is not strained and, hence, the bonds, if broken, simply reform because local lattice relaxation does not prevent them from doing so. The suggestion of a lattice rearrangement being necessary for both the bond cleavage and anneal is consistent with the temperature dependent studies. The observation that the decay of Si^{+3} intensity is accompanied by an increase in SiO_2 intensity (figure 20) is likewise consistent with a model in which the cleaved covalent bond can simply reform, thereby repairing the SiO_2 lattice network.

V. BOND STRAIN GRADIENT (BSG) MECHANISM FOR RADIATION INDUCED INTERFACE STATE GENERATION

V.A. The Model

In this section we propose a mechanism for the formation of interface states in MOS structures exposed to ionizing radiation. This model is consistent with the experimental observations reported in sections III and IV as well as with a variety of observations reported in the literature. In section III, we provided evidence, using a variety of experimental techniques, for the existence of a structurally, but not stoichiometrically, distinct region of SiO_2 near the SiO_2/Si interface. The data are consistent with the presence of strained Si-O bonds in this near interfacial region due to the "lattice mismatch" between the crystalline silicon and the amorphous SiO_2. We furthermore observed that the amount and spatial extent of strained SiO_2 were greatest for radiation soft as compared to radiation hard gate oxides. In section IV, during the *in situ* electron stressing of gate oxides, we observed the formation and decay of a Si 2p signal consistent with a Si atom in the +3 oxidation state. An oxide species consistent with this is a Si atom bonded to 3 network oxygen atoms and having a singly occupied dangling orbital (a hydrogen atom bonded to this dangling orbital is also consistent with the observed binding energy). This trivalent species will hereafter be denoted as O_3-Si· for convenience. Based on the observation of a O_3-Si· site following electron stress, we proposed that the effect of the electron stress was to break a covalent Si-O bond in the SiO_2 matrix to yield a neutral O_3-Si· species and a nonbridging oxygen site.

The observations stated above have lead us to suggest a three stage mechanism for the formation of interface states in MOS structures exposed to ionizing radiation. This mechanism is summarized in figure 22. The first step

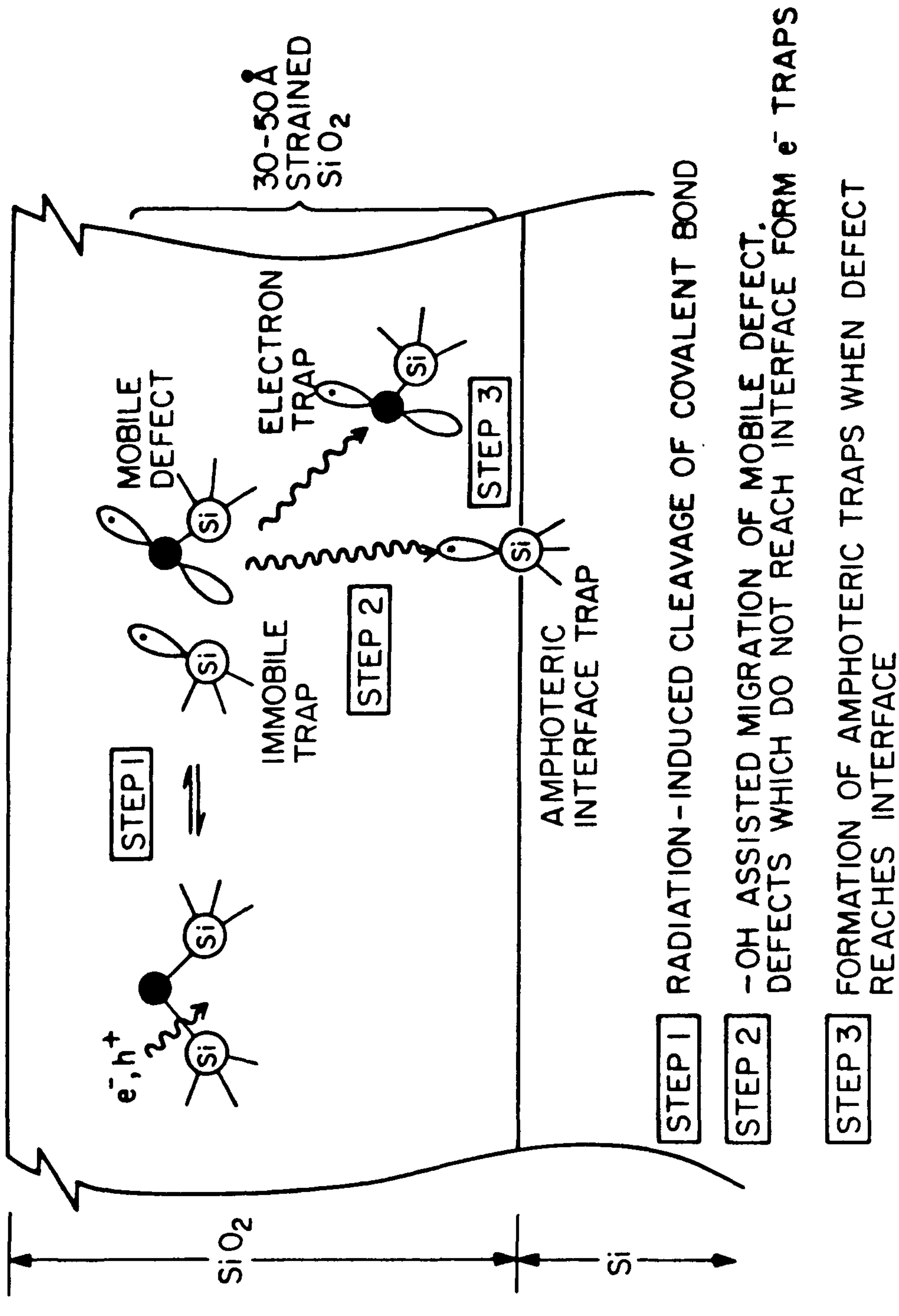

Figure 22: Summary of the proposed three-stage bond strain gradient mechanism for the formation of interface states following exposure of an oxide to ionizing radiation.

involves the cleavage of a Si-O covalent bond in the near-interfacial region of the SiO_2 to produce mobile and non-mobile defects in the oxide. Step 2 involves the migration of the mobile defect towards the SiO_2/Si interface aided by the strain gradient in the near-interfacial SiO_2. Finally, in step 3, an amphoteric trap is formed at the SiO_2/Si interface when the migration of the mobile defect is terminated at the Si surface. A detailed discussion of each of these steps is provided in the sections below.

V.A.1 Step 1: Radiation-Induced Cleavage of a Si-O Covalent Bond

The details of this step have previously been discussed in section IV.C and are summarized in figure 21. The rupture of a Si-O covalent bond results in two species: (1) a non-bridging oxygen defect and (2) a O_3-Si· species. This aspect of the model is essentially that proposed by Greaves.[13] Relaxation of the local lattice prevents the covalent bond from simply reforming, as originally suggested by Arnold and Compton[14] and by Nelson and Crawford.[15] The O_3-Si· species is a stationary defect held immobile because of bonding to the network oxygen. The non-bridging oxygen defect, however, is mobile and responsible for subsequent lattice rearrangement as discussed in steps 2 and 3.

V.A.2 Step 2: Hydroxyl Assisted Migration of the Non-bridging Oxygen Defect

The second stage of this mechanism involves the rapid movement of the non-bridging oxygen defect via a low energy rearrangement process. This mechanism was originally proposed by Fratello, et al., for the devitrification of fused silica and subsequent formation of quartz.[16] In the mechanism proposed by Fratello, et al., a non-bridging oxygen defect resulting from a broken Si-O bond and its association with a hydroxyl group permit the crystallization of quartz from a vitreous silica network. As illustrated in figure 23, the cooperative motion of the nonbridging oxygen and the highly mobile OH group results in the crystallization of a row of molecules along a crystalline/amorphous interfacial ledge. They propose that the active site consists of an OH group attached to the same Si atom as the non-bridging oxygen as shown in figure 23a. In figure 23b, this mobile defect approaches another Si atom where the simultaneous breaking and forming of bonds results in the migration of the non-bridging oxygen defect to a new site. The OH group can also transfer to this new site via a low energy exchange mechanism (10-20 kcal/mole) while the two Si atoms are in close proximity (figure 23c). Additional lattice relaxation deforms the SiO_2 rings toward another rearrangement (figure 23d-e). Continuation of this rearrangement process results in the crystallization of quartz along the crystalline/amorphous ledge. The increased strain at the crystalline/amorphous boundary tends to keep the propagation of defects along this ledge. Fratello and coworkers have experimentally verified the necessity of the OH group in that they observe that the rate of quartz crystallization from silica extrapolates to zero in the absence of OH. They suggest that the association of OH with the non-bridging oxygen defect provides an added degree of freedom in the motion of this site since its presence releases the defect from one of the network oxygen atoms.

The model by Fratello and coworkers discussed above may be straightforwardly adapted to amorphous SiO_2 on Si. Here we suggest that the strain boundary now becomes the strain gradient we observe in the near-interfacial SiO_2. Figure 24 illustrates the migration process within the amorphous SiO_2 network. The non-bridging oxygen atom with its singly occupied orbital is attracted towards a nearby Si atom. A five-coordinate transition complex results. The existence of five-coordinate intermediate complexes for silicon is well established

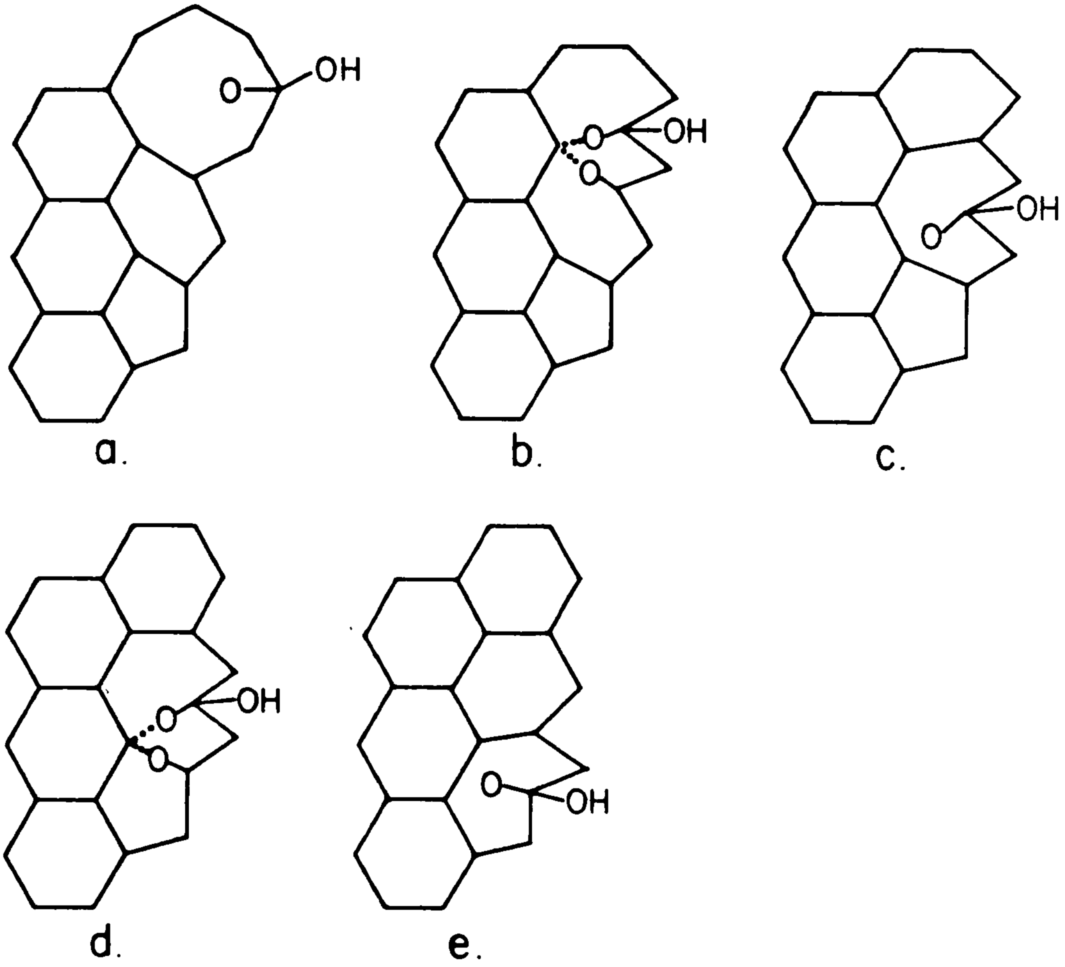

Figure 23: Schematic representation of defect propagation for the growth of quartz crystals in fused silica. Mechanism from reference 6.

STEP 2 OH ASSISTED MIGRATION OF NON-BRIDGING OXYGEN DEFECT

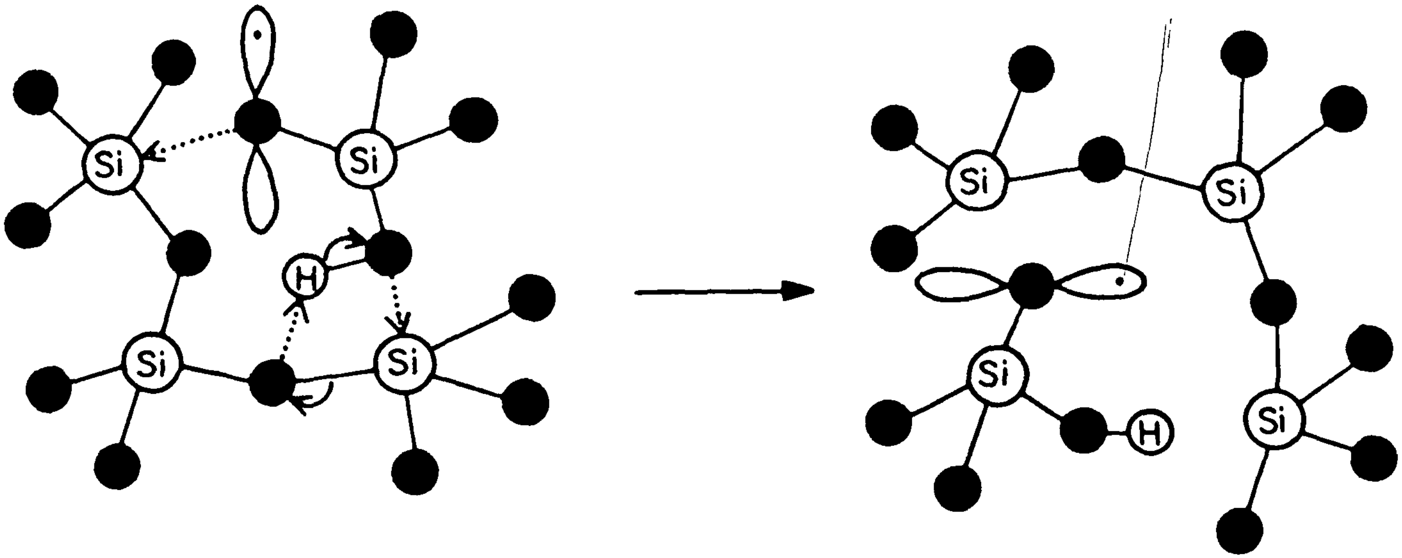

Figure 24: Illustration of step 2 of the proposed three-stage bond strain gradient mechanism, demonstrating the OH assisted migration of the non-bridging oxygen defect.

in the chemical literature[17] and is possible because of the empty d orbitals on the Si atom. Virtually simultaneously with the formation of this fifth Si-O bond, the weakest of the Si-O bonds in the complex breaks. The result is that the non-bridging oxygen defect is now on a different Si atom site. Notice in figure 24 that the oxygen atom itself does not migrate; only the defect effectively migrates. Also shown in figure 24 is the accompanying migration of the OH group. It moves via a very similar low energy bond make/break process. Notice again, that the OH group itself is not migrating, but that only the hydrogen atom is moving from site to site. Because the Si-O bonds become increasingly strained towards the SiO_2/Si interface, the migration process in figure 24 will proceed in the direction of the interface. Crystallization of the amorphous SiO_2 as the non-bridging oxygen defect propagates toward the interface, similar to the devitrification of silica observed by Fratello, et al., would seem to be unlikely since the strain boundary is along an amorphous/amorphous ledge rather than along a crystalline/amorphous ledge as studied by Fratello, et al. It is interesting, however, that microcrystallites of crystabolite have been observed in amorphous SiO_2 on Si using transmission electron microscopy.[18] We suggest that these crystallites are precipitating in the SiO_2 network via the strain-releasing mechanism discussed above.

V.A.3 Step 3: Formation of Amphoteric Traps at the SiO_2/Si Interface

Figure 25 illustrates the termination of the non-bridging oxygen defect migration at the SiO_2/Si interface. Because a Si-Si bond is weaker than a Si-O bond, the attack of the non-bridging oxygen atom on a Si atom bonded to another substrate Si atom will result in the breaking of the Si-Si bond. The result is that the singly occupied orbital is now present on a substrate Si atom rather than on another oxygen atom in the oxide network. The defect is no longer mobile since

STEP 3 FORMATION OF AMPHOTERIC TRAPS WHEN MIGRATION OF DEFECTS TERMINATE AT SiO_2/Si INTERFACE

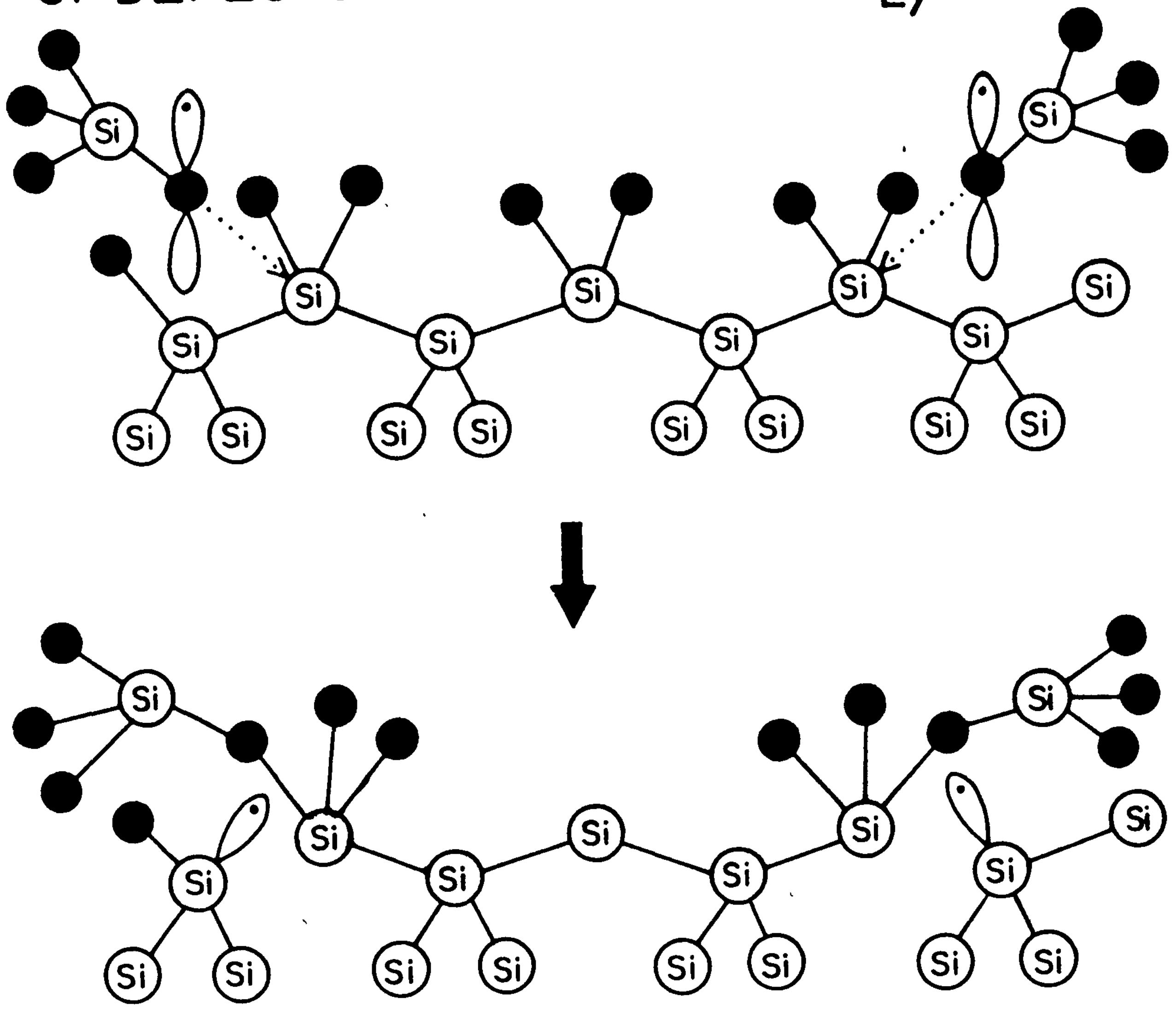

Figure 25: Schematic of step 3 of the proposed three-stage bond strain gradient mechanism, illustrating the formation of amphoteric traps at the SiO_2/Si interface.

this species is held rigid by the substrate lattice. As illustrated in figure 25, the termination of the non-bridging oxygen defect at the substrate can result in several interfacial species, depending upon the type of interfacial site attacked. This figure illustrates the formation of a Si atom with a singly occuped orbital and bonded to 3 other Si atoms in the substrate (Si_3-Si·), as well as a partially oxidized site in which one of the substrate atoms is replaced with a network oxygen (Si_2O-Si·). The presence of the Si_3-Si· site at the SiO_2/Si(111) interface has been determined using electron paramagnetic resonance (EPR)[19] and a correlation has been established between this species and radiation-induced interface states.[20,21] A Si_2O-Si· site has likewise been tentatively assigned in the EPR spectra for SiO_2/Si(100) interfaces.

The examination of figure 25 suggests that the distribution of intermediate oxidation states of silicon in the transition layer between SiO_2 and Si is quite important in establishing the termination products of the mobile non-bridging oxygen defect. For example, to form the EPR observed Si_3-Si· site on Si(111), the non-bridging oxygen must attack a Si_2O_3 site at the interface. For formation of the EPR observed sites Si_3-Si· and Si_2O-Si· on Si(100), both Si_2O_3 and Si_2O sites are important. This issue will be discussed in more detail in section VI, where the suboxide distributions for hard and soft gate oxide processing conditions are reported.

V.A.4. Relationship of Model to Other Observations

The model discussed above for interface state formation is consistent with our experimental observations as well as with a number of observations within the literature. First, we observe that the strained SiO_2 region extends farther away from the interface in soft oxides as compared to hard. Thus, a Si-O bond in the soft oxide broken anywhere within the strained regime will result in the propagation of the defect towards the interface and the formation of an interface state. In constrast, bonds broken within a hard oxide have a reduced probability of occuring within the strained region, and will therefore tend to either reform or remain in place.

It has been demonstrated that there is an enhanced buildup of fixed positive charge and interface states for wet oxides as compared to dry oxides.[22] We observe that the strain region in wet oxides is essentially the same as that in dry oxides. Therefore, we suggest that wet oxidation does not result in a greater strain in the network oxide, but rather simply provides for more OH groups which facilitate the propagation of the non-bridging oxygen defect.

Temperature dependence studies have shown that the interface state density in MOS structures increases after samples irradiated at low temperatures are warmed to higher temperatures.[23] These results support the suggestion that lattice rearrangement is involved in the propagation of defects toward the interface. Bonds broken at low temperatures are inhibited from propagating toward the interface until the temperature is sufficiently high to allow mobility of the lattice atoms.

VI. THE CHEMICAL STRUCTURE OF THE SiO_2/Si INTERFACE: THE SiO_x TRANSITION LAYER

We describe here XPS measurements of SiO_2/Si interfaces representing contrasts between oxides grown on (100) versus (111), grown by wet and dry oxidation processes, and processed with and without a high temperature post-oxidation anneal (POA). These measurements reveal significant trends in the distribution of suboxide states among these samples.

There are five possible oxidation states for Si as illustrated in figure 26.

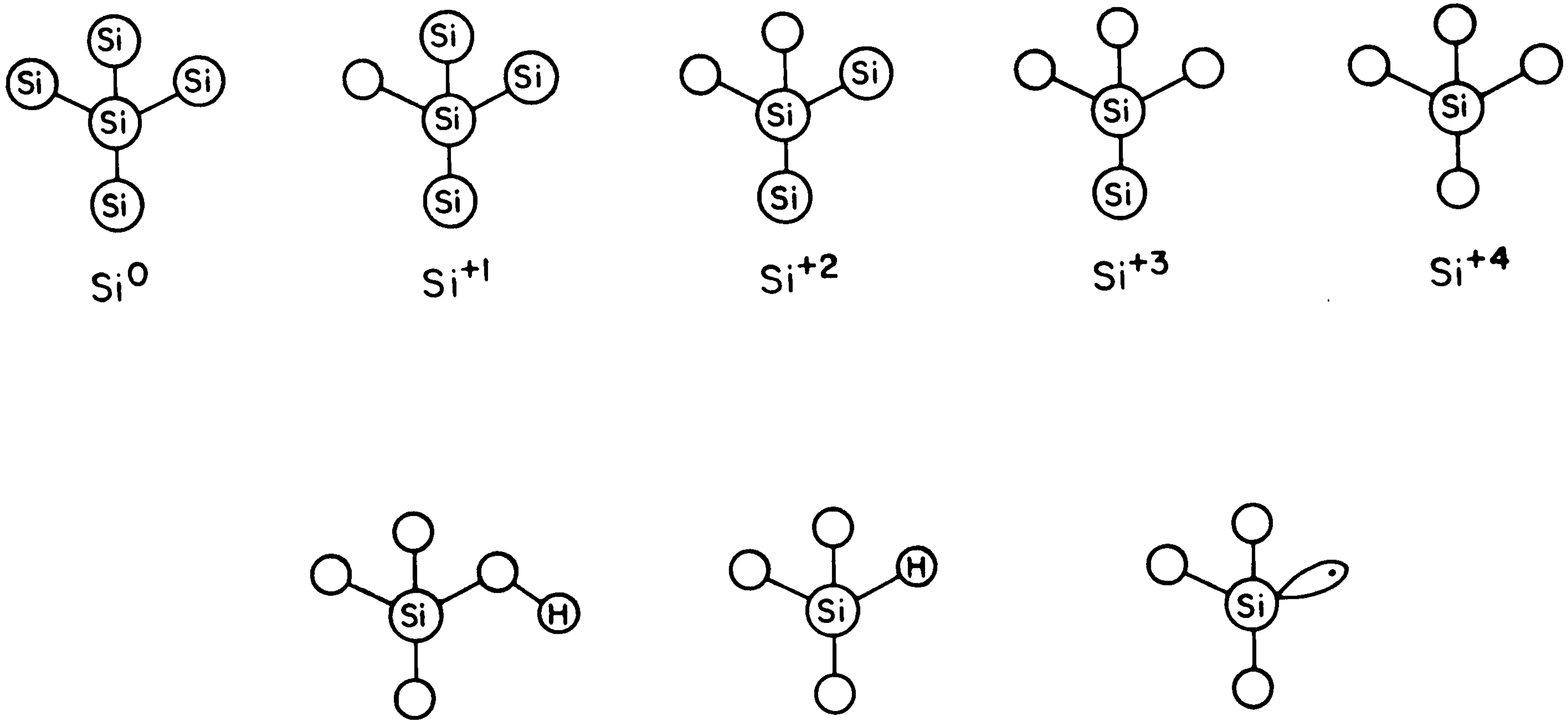

Figure 26: Illustration of the five possible oxidation states of silicon.

Elemental Si and SiO_2 are in Si^0 and Si^{+4} states, respectively. Suboxide states are characterized by bonding to 1, 2, or 3 oxygen atoms and will hereafter be referred to as Si^{+1}, Si^{+2}, and Si^{+3} states, respectively.

VI.A. Localization of Suboxide States at the SiO_2/Si Interface

In this section, we will provide evidence that the suboxide states are localized at the SiO_2/Si interface and do not extend into the bulk SiO_2. An analysis of the general problem of photoelectron attenuation by overlayers makes it possible to distinguish the case of an abrupt interface from an extended interface by plotting a normalized suboxide intensity versus oxide thickness. If the suboxides are localized at the SiO_2/Si interface, this normalized intensity will be independent of oxide thickness. Conversely, suboxides dispersed throughout the film will give a normalized intensity ratio which is a strong function of oxide thickness.

A characteristic XPS spectrum of a thin oxide on Si is shown in the upper curve of figure 27a. The doublet feature at low binding energy corresponds to the Si substrate while the broad feature at high binding energy is due to SiO_2. In the lower curve of figure 27a, the spin-orbit split component has been removed from the data to simplify analysis. Overplotted on this curve are spectra corresponding to bulk SiO_2 and Si. The shaded region corresponds to suboxide states and is shown as a difference spectrum in the upper curve in figure 27b. The positions of the suboxide states are consistent with those previously determined by resolution enhancement techniques[6] as well as with those determined using synchrotron radiation photoemission spectroscopy.[24] The intensities of the suboxide states have been determined by integrating peaks fit to the difference spectra via least squares minimization.

A representative data set calculated from the chemical depth profile of a Si

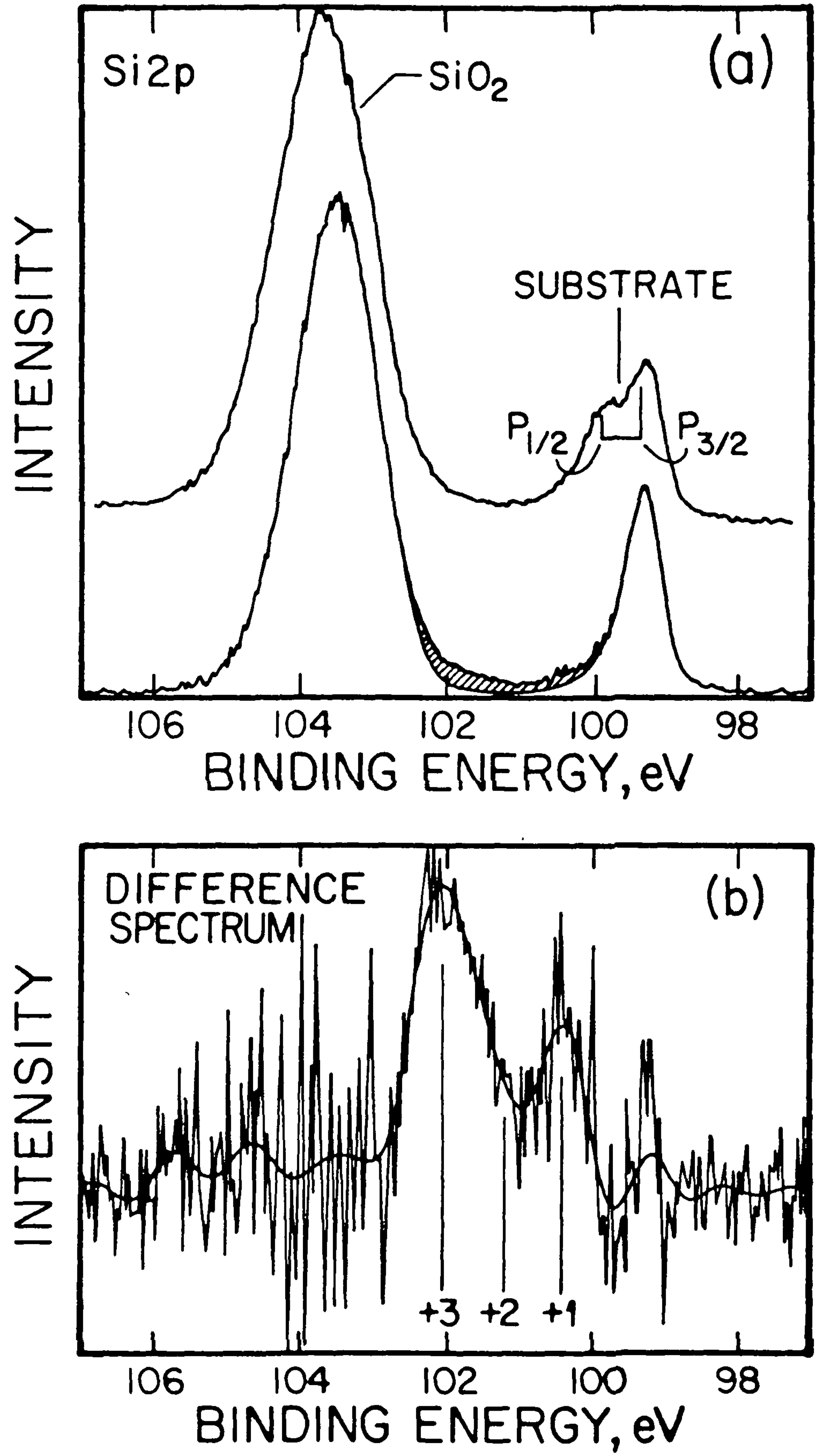

Figure 27: (a) Upper curve: the Si 2p region of a thin thermal oxide on silicon; lower curve: data from upper curve with the spin-orbit components removed. Si 2p spectra from bulk Si and SiO_2 are overplotted to emphasize the suboxide region (shaded). (b) Difference spectrum obtained by subtracting the bulk contributions from the thin thermal oxide spectrum in the lower curve in (a).

(100) substrate oxidized in steam at 900^{o} C followed by a 1150^{o} post-oxidation anneal in N_2 is given in figure 28. Note that the x axis can only be expressed as the ratio of the actual oxide thickness to the average mean free path, $<\lambda>$. We have observed consistently that the mean free path is a strong function of local chemistry and obtained λ values for SiO_2 ranging from 24 to 36 Å. Assuming a value for λ of 36 Å, the scale of intensities plotted in figure 28 represents the first 10 - 15 Å out into the oxide from the interface. We have resolved the total SiO_2 signal into the strained and unstrained components. The strained component is distributed near the interface and appears to peak at 15 Å for this sample condition. The Si^{+1}, Si^{+2}, and Si^{+3} species show no oxide thickness dependence. This is emphasized by the expansion of figure 28 given in figure 29. Within experimental error, the Si^{+2} and Si^{+1} intensity ratios for oxide thicknesses greater than 4-6 Å show no functional dependence on oxide thickness. We can therefore conclude that the Si^{+1} and Si^{+2} species are localized at the interfacial monolayer. The Si^{+3} signal shows a modest dependence to a thickness of 10 to 15 Å from the interface. We have attributed this to the presence of two Si^{+3} species: (1) a Si^{+3} species immediately at the SiO_2/Si interface (a Si atom bonded to 1 substrate Si atom and 3 oxygen atoms) and (2) a Si^{+3} species due to hydrogen bonding in the SiO_2 (a Si atom bonded to 1 hydrogen atom and 3 oxygen atoms). Note also in figure 29 that the normalized intensity of each suboxide species falls off drastically for oxide thicknesses less than 4 to 6 Å. We suggest that this thickness corresponds to that point at which the etchant penetrates the suboxide layer and begins direct removal of these species. The total number of suboxide species observed at an oxide thickness of $0.15<\lambda>$ (approximately 1 monolayer) corresponds to 5.4×10^{14} cm^{-2}, which suggests 0.8 of an interfacial monolayer can be accounted for by suboxide species. Our previous assignment of an interfacial width of 5 - 7 Å

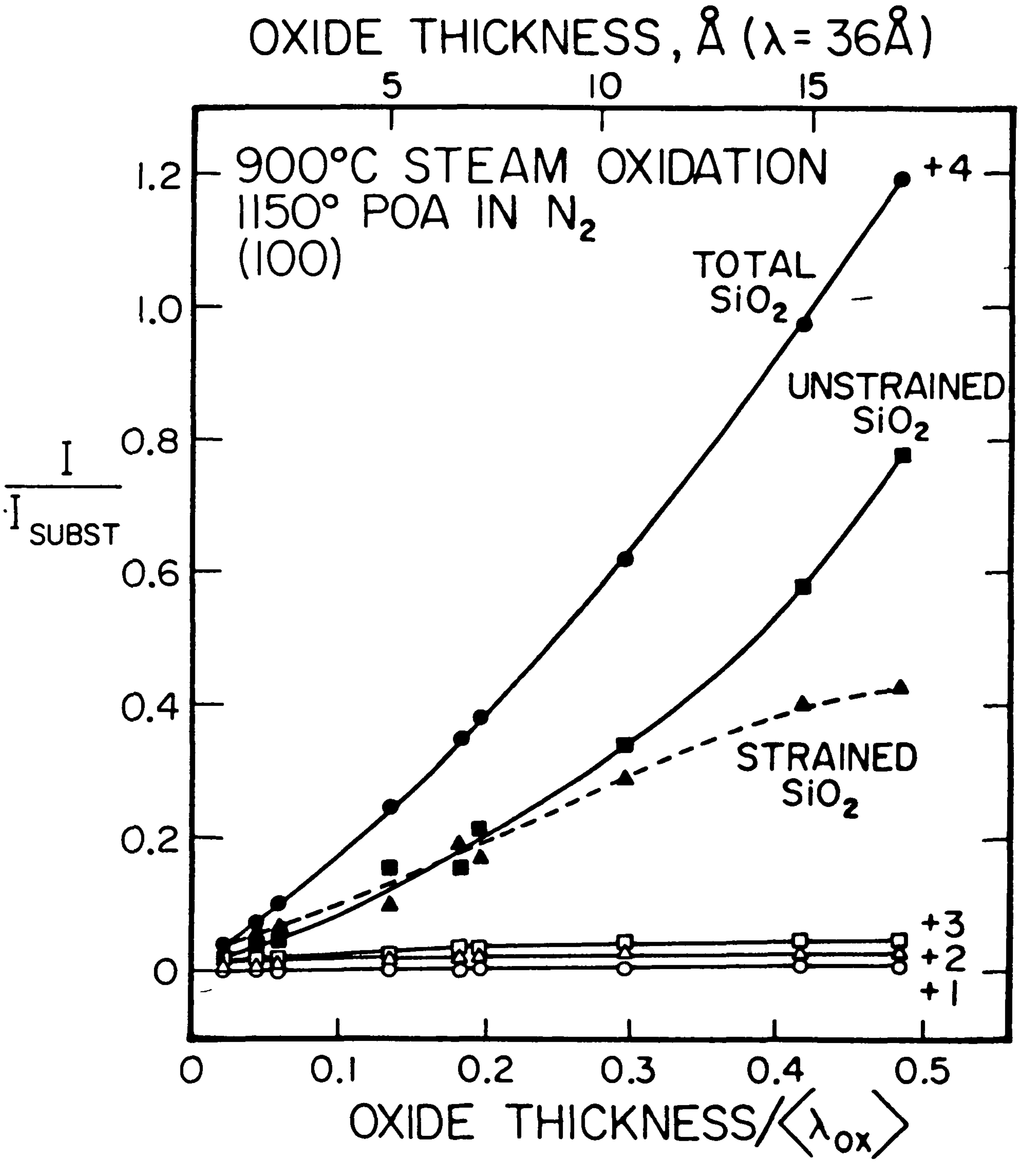

Figure 28: Normalized Si 2p intensities of the oxide and suboxide components plotted against a reduced average oxide thickness for a chemical depth profile of a thermal oxide on Si (100).

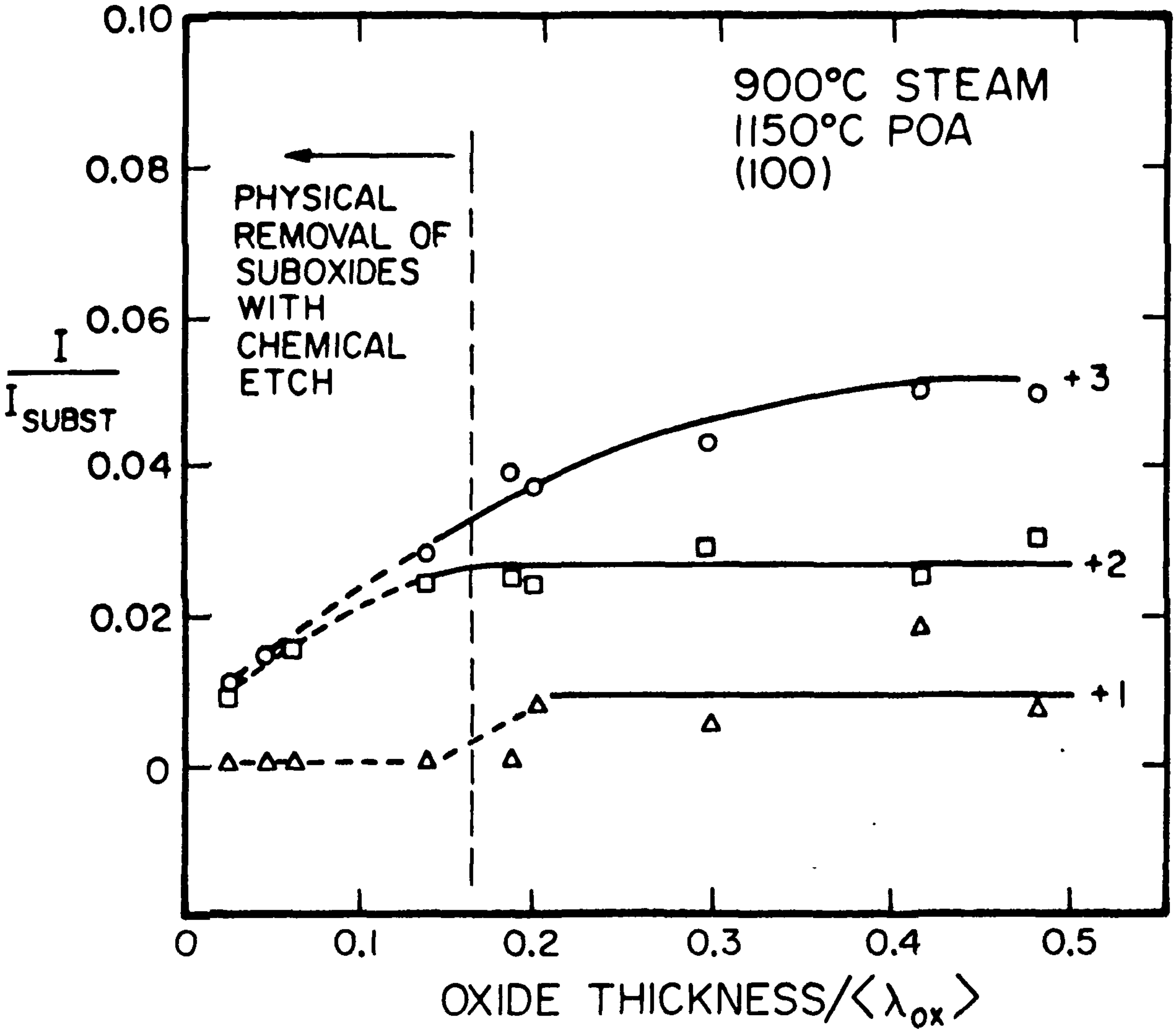

Figure 29: Expansion of the vertical scale in figure 28, emphasizing the suboxide contributions.

(approximately one monolayer) in thermal oxides is based on our reproducible observations of a well-defined etching threshold for suboxide removal. This thickness is derived from attenuation of the substrate photoelectron signal. Analysis of the absolute suboxide intensity suggests that only 75 to 85% of a monolayer of suboxides is present at the interface. To make these numbers self-consistent, one needs to postulate that the remaining 15-25% of a monolayer at the interface that is not attributable to suboxide species is associated with bonding to impurity species (H, C, F).

VI.B. Crystallographic Dependence and Interfacial Roughness

The composition of the interfacial transition layer should be a strong function of the crystallographic orientation of the substrate. On an ideal unreconstructed Si(100) surface, each Si atom has two unsatisfied bonds and should form only Si^{+2}. On a Si(111) surface, each Si atom has either one or three unsatisfied bonds, depending upon the plane terminating at the surface. These ideal interfaces are illustrated in the upper panel of figure 30. The actual interface, however, consists of a number of monolayer and possibly multi-monolayer steps. As illustrated in the lower panel of figure 30, we suggest that step edges, kinks, and impurity sites will give rise to different suboxide distributions than those ideally anticipated. This orientation dependence of the suboxides is illustrated for Si (111) and Si(100) substrates in figures 31 and 32, which plot normalized intensity ratios for the suboxide species as a function of oxide thickness. As shown in figure 31, virtually no Si^{+2} can be detected at the SiO_2/Si(111) interface. Conversely, as shown in figure 32, virtually no Si^{+1} can be detected at the SiO_2/Si(100) interface. Si^{+3} species can be detected at both (100) and (111) interfaces, but, as discussed earlier, we believe that this signal is due in part to the presence of Si-H bonding

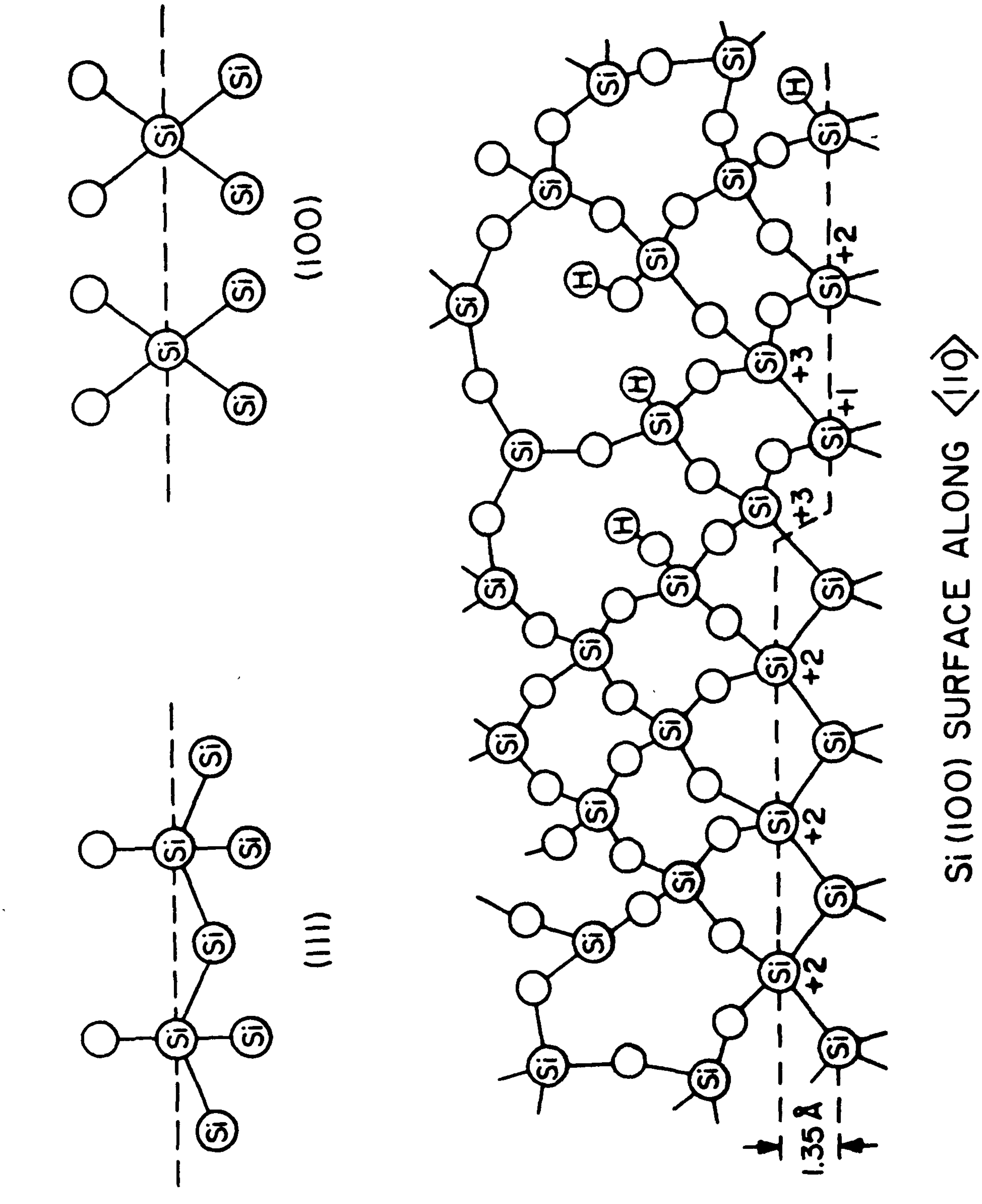

Figure 30: Idealized diagram of local atomic interface geometry.

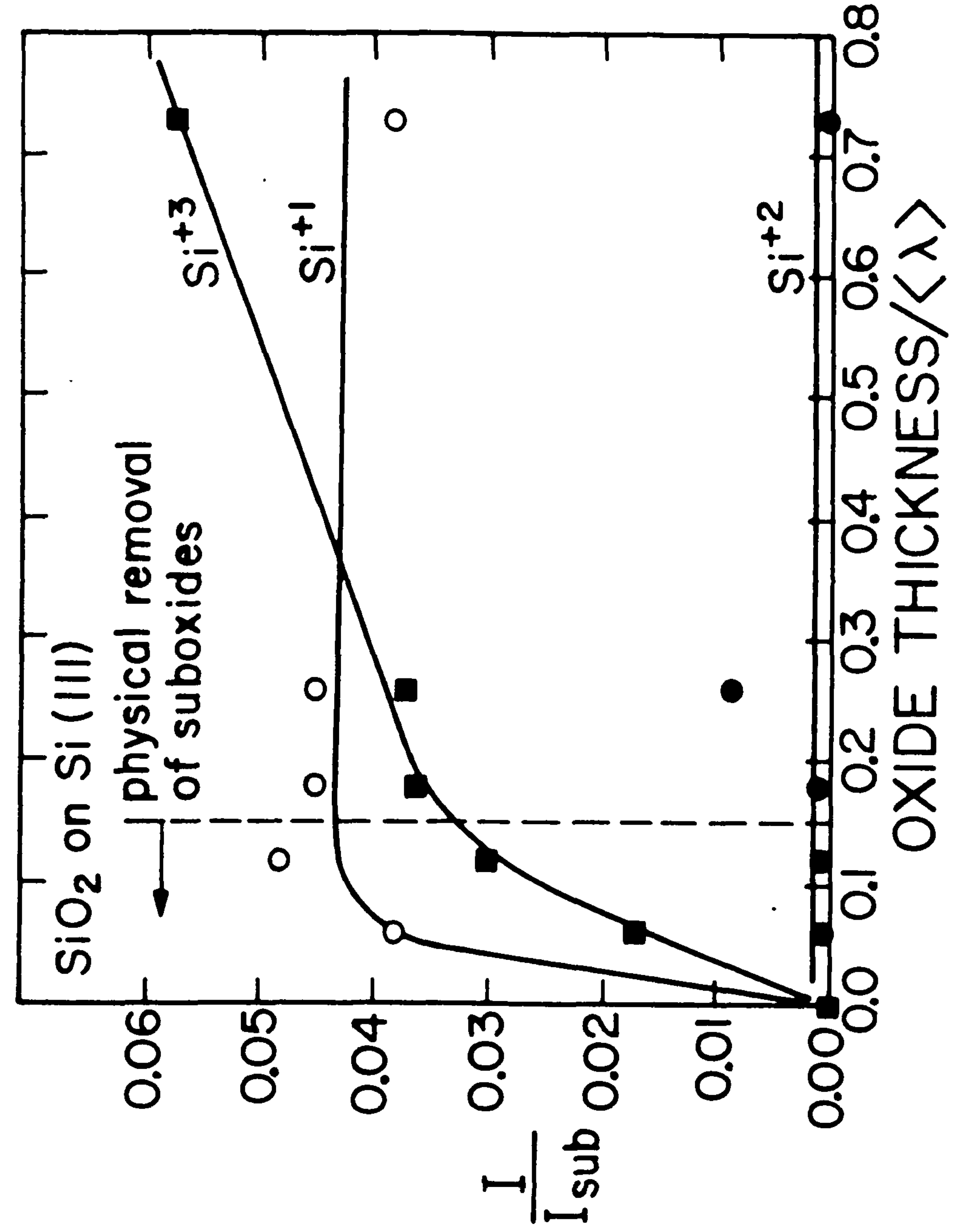

Figure 31: Normalized Si 2p suboxide intensities versus a reduced average oxide thickness for a dry thermal oxide on Si (111).

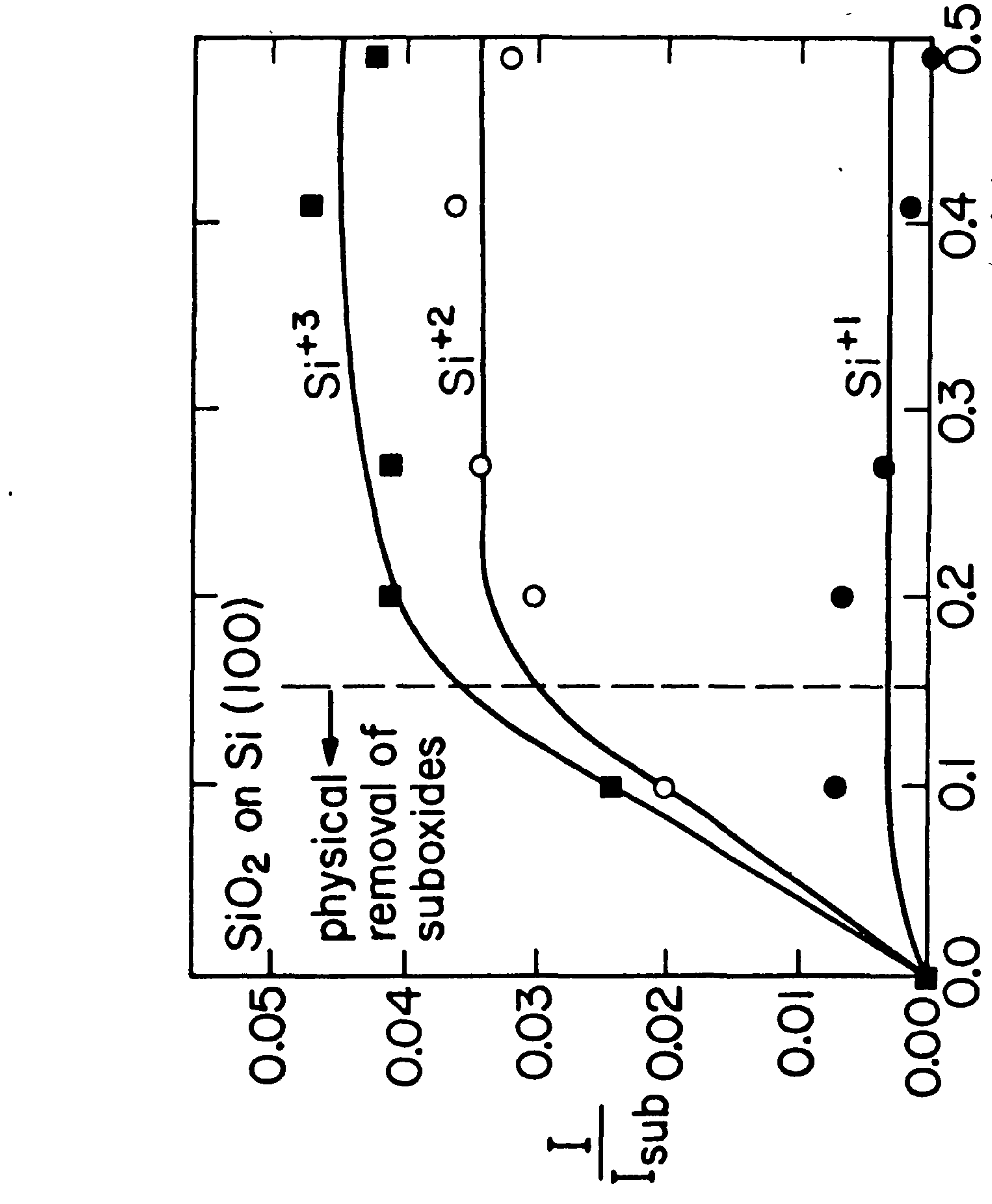

Figure 32: Normalized Si 2p suboxide intensities versus a reduced average oxide thickness for a dry thermal oxide on Si (100).

within the SiO_2 which should not show any crystallographic dependence. Based on these results, we suggest that the extent to which suboxides other than Si^{+1} on (111) or Si^{+2} on (100) occur is a measure of the local atomic roughness and impurity sites at the intact interface. In this experiment, a thin oxide layer can remain to preserve the interfacial structure. This is in contrast to the method of Hahn and Henzler[25] which analyzes interfacial roughness by measurement of the specular spot profile in high resolution LEED and requires the complete removal of the oxide overlayer.

VI.C. Process Dependence: Post-Oxidation Anneal Temperature

In an effort to establish a correlation between the chemical structure of the interface and the electronic properties of the SiO_2/Si system, we have examined the effect on interfacial composition of a high temperature (1150° C) post-oxidation anneal (POA) in a N_2 ambient. This procedure typically leads to a substantial increase in the susceptibility of the oxide structure to interface state formation and increased fixed positive charge after ionizing radiation exposure. The suboxide distributions for a wet oxidation process for Si (100) are given in the histogram in figure 33. Note the deviation away from an ideal interface as evidenced by the increase in Si^{+1} and decrease in Si^{+2} after the POA. These results suggest a roughening of the interface following a high temperature POA. The Si^{+3} intensity shows only a modest increase in intensity, but the interpretation of this signal is complicated by the presence of Si-H species in the oxide as mentioned earlier. The suboxide distributions for wet and dry processes are similar in that both suggest a roughening of the interface following a high temperature POA. The increased radiation susceptibility of MOS structures following a high temperature POA suggests a correlation between interface states and terrace edges or kink

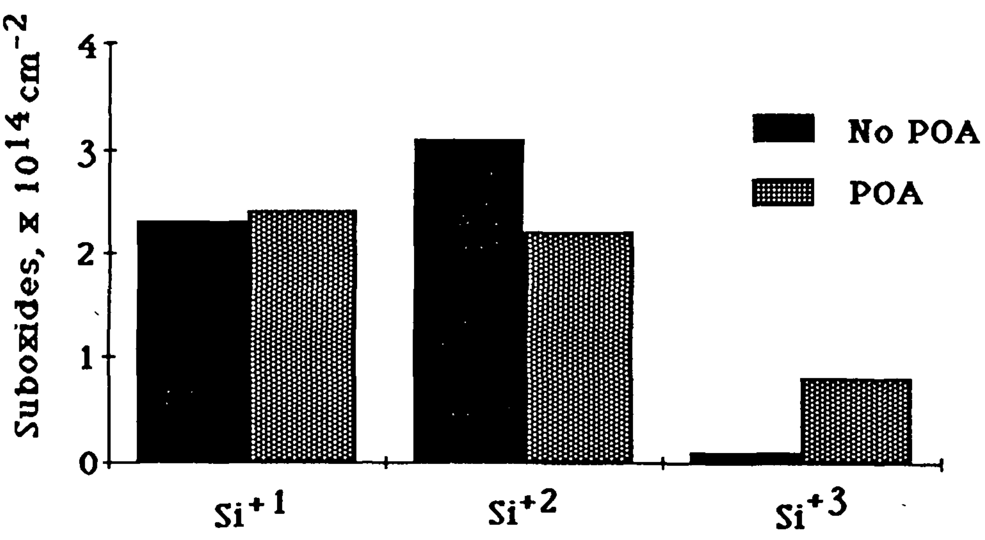

Figure 33: Summary of suboxide intensities for a pyrogenic thermal oxide (850 Å thick) comparing the effect of a 1150° C post-oxidation anneal versus no anneal.

the interface.

These results would appear to be in conflict with the results of Hahn and Henzler,[25] who concluded that a POA smooths the interface. However, the POA described by Hahn and Henzler was perfomed at the same temperature as the oxidation (1000° C), while in the present work the POA was at a signficantly higher temperature (1150° C). These results suggest that a low temperature POA smooths the interface, while a high temperature POA roughens the interface.

VI.D. Implications for the BSG Mechanism

In our studies of radiation induced damage in MOS gate dielectrics, we have suggested that the hole-induced cleavage of strained Si-O-Si bonds gives rise to non-bridging oxygen defects and trivalent Si^{+3} centers in the oxide (see section IV). We have proposed that non-bridging oxygen species are mobile and can follow the oxide strain gradient in the near interfacial region of the oxide and be transported to the oxide interface. Reaction of a non-bridging oxygen center with an interfacial suboxide can generate an EPR active dangling bond site which has been shown to correspond to an electrically active interface state. This mechanism for radiation induced interface state generation has been discussed previously in section V and is illustrated in figures 21-25. The particular kind of dangling bond center formed during the non-bridging oxygen center reaction depends on the silicon suboxide encountered at the interface. Analysis of the structural chemistry suggests that the Si^{+3} site is a rather unique entity at the interface. Reaction with this site will create a center similiar to that observed by EPR. Furthermore, such a reaction will lead to local oxide strain relief at the site of the dangling bond center formed because, as illustrated in figure 34, the original Si^{+3} site is completely released from its bonding to substrate Si atoms. It is therefore intriguing to

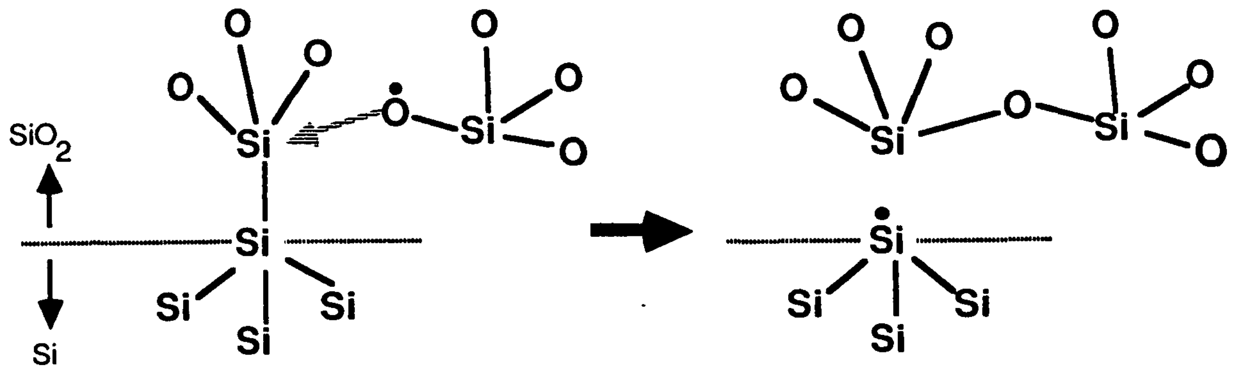

Figure 34: Schematic of the reaction between a non-bridging oxygen defect and a Si^{+3} site at the SiO_2/Si interface.

speculate that increased atomic roughness at the interface will lead to a higher population of interfacial Si^{+3} sites and to a correspondingly higher probability of interface state formation during ionizing radiation stress.

VII. CONCLUSIONS

The objective of this task was to obtain chemical and structural information on the SiO_2/Si interface in MOS samples fabricated at the Sandia Laboratory. These samples were specifically designed to isolate the key processing requirements for radiation hard MOS device structures. Photoemission spectroscopy was used to examine the near-interfacial region of SiO_2 as well as the immediate SiO_x transition layer in radiation hard and soft oxides. These experiments reveal significant trends in the chemistry and structure of the SiO_2/Si interface for MOS structures with differing degrees of susceptibility to damage by ionizing radiation.

The major accomplishments of this task are sixfold:

1. *The identification of a structurally distinct region of SiO_2 in the near-interfacial region of thermal SiO_2 on Si.*

Evidence for the existence of a structurally distinct region of SiO_2 near the SiO_2/Si interface was derived from four distinct experiments: (i) analysis of XPS Si 2p binding energies; (ii) analysis of XPS Si 2p intensities; (iii) chemical etch rate differences, and (iv) SEXAFS measurements. Collectively, these experiments demonstrate conclusively that the first 30-50 Å of SiO_2 at the SiO_2/Si interface are structurally distinct from bulk SiO_2. We have provided evidence that this distinction is due to a shift in the distribution of Si-O-Si bridging bond angles within the SiO_2 network towards smaller angles near the interface as compared to bulk SiO_2. This shift in the distribution of bridging bond angles has signficant implications regarding the network structure of the near-interfacial SiO_2. SiO_2 is known to consist of SiO_4 tetrahedrons linked together by shared oxygen atoms to form a network ring system. The smaller the bridging bond angle, the fewer the number of tetrahedrons that may be linked within a ring. Our data support a picture in which the SiO_2 interconnecting ring network in the near-interfacial region is comprised of significantly smaller rings than those found in the bulk SiO_2. This decrease in the average bond angle in the near-interfacial region is a natural consequence of the "lattice-mismatch" between SiO_2 and crystalline Si.

2. *The identification of structural differences between radiation hard and soft gate oxides in the near-interfacial SiO_2 region.*

We have demonstrated using fixed and variable photon energy photoemission spectroscopy that the *spatial* extent of the structurally distinct SiO_2 region near the SiO_2/Si interface (discussed above) is different for radiation hard versus soft oxides. Specifically, we find that the spatial extent of the near-interfacial SiO_2 is considerably larger for soft gate oxides. Because the smaller bond angles found in the near-interfacial SiO_2 are strained relative to bulk SiO_2, these results have important implications for the formation of interface states following exposure of the oxide to ionizing radiation.

3. *The direct observation of radiation-induced damage sites in thermal SiO_2.*

In situ electron irradiation experiments were performed in conjunction with XPS to study the effect of ionizing radiation on the network structure of thermal SiO_2 on Si. A damage peak consistent with a Si^{+3} state was observed to appear after irradiating SiO_2 with electrons of sufficient energy to create holes via impact ionization. The production and decay of this damage signal were monitored as a function of oxide thickness and sample temperature. The data are consistent with the radiation-induced cleavage of a Si-O covalent bond within the SiO_2 network. The products of this cleavage are (i) a Si^{+3} species (a Si atom bonded to three network oxygen atoms and having a singly occupied dangling orbital) and (ii) a Si^{+4} species (a Si atom bonded to three network oxygen atoms and one nonbridging oxygen atom).

4. *The correlation of suboxide distributions at the SiO_2/Si interface with radiation susceptibility.*

XPS has been used to examine the incomplete oxidation states at or near the SiO_2/Si interface. We find that all three suboxide states (Si^{+1}, Si^{+2}, and Si^{+3}) are localized within the first monolayer at the SiO_2/Si interface. A small component of the Si^{+3} states extend 10-15 Å into the oxide, which we attribute to hydrogen bonds in this region. A study of the crystallographic dependence of the suboxide distribution suggests that the extent to which suboxides other than Si^{+1} on (111) or Si^{+2} on (100) occur is a measure of the local atomic roughness (steps) and impurity sites at the interface. In comparing the suboxide distributions for hard and soft oxides, we find that there is a large increase in Si^{+1} and decrease in Si^{+2} for soft as compared to hard. These results suggest that atomic roughening of the interface occurs when a hard oxide is softened by a high temperature post-oxidation anneal. This correlation suggests a link between interface states and terrace edges or kink sites at the interface.

5. *The development of a chemical mechanism for radiation-induced interface state generation in SiO_2/Si structures.*

The observations in *1* through *4*, above, have led us to suggest a three stage mechanism for the radiation-induced formation of interface states in MOS structures. The first step involves the cleavage of a Si-O covalent bond in the near-interfacial region of the SiO_2 to produce a nonmobile Si^{+3} species and a mobile Si^{+4} non-bridging oxygen defect. The second step involves the hydroxyl assisted migration of the non-bridging oxygen defect towards the SiO_2/Si interface, aided by the strain gradient in the near-interfacial SiO_2. In the final step, an amphoteric trap is formed at the SiO_2/Si interface when the mobile defect reacts with the Si surface. A detailed description of and supporting evidence for the mechanism are provided. We speculate upon how the above mechanism provides a basis for understanding how increased atomic roughness at the interface may lead to a higher probability of interface state formation following ionizing radiation exposure.

6. *The development of selective chemical etching techniques which permit the investigation of oxide/semiconductor structures using surface sensitive spectroscopic techniques.*

We have developed a wet chemical spin-etch approach which allows the relatively benign profiling of oxide structures. This approach permits (i) the profiling rate to be precisely controlled; (ii) uniform profiling over a sample area exceeding one square centimeter; and (iii) contamination residues far lower than those found in immersion etching. Variable photon energy photoemission studies have been performed which demonstrate that the oxide structure is not affected in any measureable way by the profiling technique.

We have implemented a gas phase XeF_2 etching system to permit the benign removal of polysilicon gate electrodes in order to permit spectroscopic study of the underlying gate oxide. We have furthermore developed benign etches for the removal of Al gate electrodes which avoid the oxide contamination problems plaguing conventional Al solution etches.

VIII. RECOMMENDATIONS

The work reported here represents a careful examination of the chemistry and structure of the SiO_2/Si interfacial region for radiation hard and soft oxides. The results suggest several follow-up research efforts.

The oxides studied in this task have been subjected to standard processing conditions up to the point of gate electrode metallization. Although we received samples with both polysilicon and Al gate metallization and implemented the techniques necessary for the removal of these electrode materials, termination of this task prevented a spectroscopic study of the effect of the metallization process on the gate oxide chemistry and structure. We consider this an important area for investigation, particularly in light of our recent spectroscopic investigation of the Al/SiO_2 interface.[26,27] In these studies we observed an atomically abrupt interface between resistively evaporated Al and thermal SiO_2 prior to annealing. Post-metallization annealing, however, induces reduction of the SiO_2 by the aluminum, resulting in a complex extended interfacial region. Although the Al/SiO_2 interface is rather distant from the SiO_2/Si interface, its influence on the SiO_2/Si interfacial properties may be significant. Indeed, it has been reported that the density of radiation-induced interface states depends not only upon the conditions of the Al gate process,[28] but also upon the specific gate material used.[29] We suggest that the influence of the metallization process on the near-interfacial SiO_2

structure as well as on the distribution of suboxides at the immediate SiO_x transition layer be examined.

The results and models discussed in this report suggest several different approaches for reducing the susceptibility of an oxide to damage by ionizing radiation. First, we have observed that the spatial extent of strained SiO_2 near the SiO_2/Si interface is largest for soft as compared to hard oxides. The obvious implication is that radiation-induced interface state formation may be minimized by minimizing the extent of strained SiO_2 via manipulation of the oxide processing conditions. However, we feel that although there exists a significant difference in the amount of strained SiO_2 near the interface for hard versus soft oxides, this difference is not crucial in establishing the radiation susceptibility of the oxide. Even allowing for a generous factor of two in the difference between the volumes of strained SiO_2 hard and soft oxides, it does not seem reasonable that this alone can explain differences in the density of radiation-induced interface states of several orders of magnitude. In addition, the extent of the strained SiO_2 is only 30 to 50 Å in width. This corresponds to approximately 5 to 10 ring cage units within the SiO_2 network. It is conceptually difficult to imagine accommodating the "lattice-mismatch" between the amorphous SiO_2 and the crystalline Si substrate within a region significantly less than 5 ring cage units without creating a region of severe stress or bond strain.

The bond strain gradient mechanism suggests a second approach for reducing radiation-induced interface state formation. Once the strained Si-O bond within the SiO_2 network is cleaved by the capture of a hole (or electron), the resulting non-bridging oxygen defect will diffuse toward the SiO_2/Si interface to produce interface states as detailed in section V. Since decreasing the volume of strained SiO_2 does not appear feasible, as discussed above, the BSG mechanism suggests that inhibiting the diffusion of the non-bridging oxygen defect will decrease the formation of interface states. There are conceptual schemes for attempting this provided by the polymer and catalytic chemistry literature. It has long been known that the molecular weight degradation of siloxane polymers, which is believed to occur via a mechanism similar to that proposed for the diffusion of the non-bridging oxygen defect in the BSG mechanism, can be inhibited by the inclusion of certain organic groups at strategic points within the polymer. Similar groups may be incorporated within the SiO_2 network to interrupt the diffusion of the mobile defect to the SiO_2/Si interface. Of course, one is faced with the possibility that the inhibiting groups themselves will be detrimental to the electrical characteristics of the oxide. Nevertheless, we feel this approach merits some consideration for the reduction of radiation-induced interface states. Indeed, we have speculated that the increased radiation hardening reported for nitrided oxides may be due to the interruption of the diffusion of the non-bridging oxygen defect when it encounters a Si-N bond within the dielectric network.

Finally, we observed a striking correlation between the atomic roughness at the SiO_2/Si interface and the radiation susceptibililty of the oxide. Because the difference in interfacial roughness between a radiation hard and soft oxide constitutes the largest structural difference we have observed (recall from section VI.C that we observed a 10-fold increase in Si^{+1} states for soft as compared to hard oxides), we feel this correlation should be examined in greater detail. In our BSG mechanism, the particular kind of dangling bond center formed when the non-bridging oxygen defect terminates at the SiO_2/Si interface depends upon which silicon suboxide state is encountered. Thus, both experimental observations and our proposed mechanism suggest that the precise suboxide distribution at the interface plays a significant role in the formation of radiation-induced interface states. Although the precise measurement of interfacial roughness is a subject that has only recently received attention, work has already begun to appear in the literature identifying those processing parameters which strongly affect the density of atomic steps at the interface.[25] In addition to controlling the oxidation conditions for minimum interfacial roughness, it may be possible to smooth interfacial roughness with post-oxidation anneals under suitable ambients. Finally, in our recent work examining the interfacial roughness produced by various accepted procedures for cleaning the Si substrate prior to oxidation,[30] we find that not only do different cleaning procedures lead to significant differences in the magnitude of interfacial atomic roughness between the substrate and the native oxide remaining after the clean, but that the interfacial roughness persists even after oxides of 100 Å thickness are grown. These results suggest that not only are the conditions of oxidation important for minimizing interfacial roughness, but that the initial cleaning chemistry is extremely important as well. The latter consideration may become particularly important for the production of very thin (less than 200 Å) radiation hard gate oxides.

In final summary, we feel that continued support of fundamental research on the structure and chemistry of the SiO_2/Si interface is of critical importance for the development of radiation hard gate oxides. Although engineering approaches may develop solutions to immediate processing problems, a fundamental understanding of the relationship between the microscopic chemistry of the interface and such electrically important quantities as interface state density and fixed positive charge presents the possibility of efficiently and effectively producing gate dielectrics with the desired characteristics as device structures evolve in the long term.

IX. REFERENCES

1. F. J. Grunthaner, P. J. Grunthaner, R. P. Vasques, B. F. Lewis, J. Maserjian, and A. Madhukar, J. Vac. Sci. Technol., 16, 1443 (1979)
2. H. F. Winters and J. W. Coburn, Appl. Phys. Lett., 34, 70 (1979)
3. D. E. Ibbotson, D. L. Flamm, J. A. Mucha, and V. M. Donnelly, Appl. Phys. Lett., 44, 1129 (1984)
4. M. H. Hecht, R. P. Vasquez, F. J. Grunthaner, N. Zamani, and J. Maserjian, J. Appl. Phys., 57, 5256 (1985)
5. R. J. Bell and P. Dean, Philos. Mag., 25, 1381 (1972) and references therein
6. F. J. Grunthaner, P. J. Grunthaner, R. P. Vasquez, B. F. Lewis, J. Maserjian, and A. Madhukar, Phys. Rev. Lett., 43, 1683 (1979)
7. R. P. Vasquez and F. J. Grunthaner, Surf. Sci., 99, 681 (1980)
8. M. H. Hecht, F. J. Grunthaner, P. Pianetta, L. I. Johansson, and I. Lindau, J. Vac. Sci. Technol., A2, 584 (1984)
9. M. H. Hecht and F. J. Grunthaner, proceedings for the Society of Photo-Optical Engineers (SPIE) conference, Spectroscopic Characterization Techniques for Semiconductor Technology II, vol. 24, F. H. Pollak, ed., 1985, p 18
10. F. J. Grunthaner, B. F. Lewis, N. Zamani, J. Maserjian, and A. Madhukar, IEEE Trans. Nuclear Sci., NS-27, 1640 (1980)
11. F. J. Grunthaner, B. F. Lewis, J. Maserjian, and A. Madhukar, J. Vac. Sci. Technol., 20, 747 (1982)
12. F. J. Grunthaner, P. J. Grunthaner, and J. Maserjian, IEEE Trans. Nuclear Sci., NS-29, 1462 (1982)
13. D. L. Griscom, in The Physics of SiO_2 and its Interfaces, S. Pantelides, ed., (Pergamon Press, New York, 1978), p 232; G. N. Greaves, Philos. Mag., B37, 447 (1978)
14. G. W. Arnold and W. D. Compton, Phys. Rev., 116, 802 (1959)
15. C. M. Nelson and J. H. Crawford, J. Phys. Chem. Solids, 13, 296 (1960)
16. V. J. Fratello, J. F. Hays, F. Spaepen, and D. Turnbull, J. Appl. Phys., 51, 6160, (1980)

17. J. D. Roberts and M. C. Caserio, Basic Principles of Organic Chemistry, (W. A. Benjamin, Inc., New York, 1965) p 1180

18. F. A. Ponce, T. Yamashita, and S. Hahn, Proceedings of the Symposium on Defects in Silicon, W. M. Bullis and L. C. Kimerling, eds., The Electrochemical Society (1983)

19. P. J. Caplan, E. H. Poindexter, B. E. Deal, and R. R. Razouk, J. Appl. Phys., 50, 5847 (1979)

20. P. M. Lenahan and P. V. Dressendorfer, Appl. Phys. Lett., 41, 542 (1982); J. Appl. Phys., 54, 1457 (1983); Appl. Phys. Lett., 44, 96 (1984)

21. N. M. Johnson, D. R. Biegelson, D. M. Moyer, S. T. Chang, E. H. Poindexter, and P. J. Caplan, Appl. Phys. Lett., 43 , 553 (1983)

22. J. Maserjian and N. Zamani, J. Appl. Phys., 53, 559 (1982)

23. P. S. Winokur, H. E. Boesch, J. M. McGarrity, and F. B. McLean, J. Appl. Phys., 50, 3492 (1979)

24. G. Hollinger and F. J. Himpsel, Appl. Phys. Lett., 44, 93 (1984)

25. P. O. Hahn and M. Henzler, J. Vac. Sci. Technol., A2, 574 (1984)

26. M. H. Hecht, F. J. Grunthaner, and J. Maserjian, Mat. Res. Symp. Proc. Vol. 25, (Elsevier Science Publishing Co., Inc., 1985) p 317

27. M. H. Hecht, R. P. Vasquez, F. J. Grunthaner, N. Zamani, and J. Maserjian, J. Appl. Phys., 57, 5256 (1985)

28. M-R. Chin and T-P. Ma, Appl. Phys. Lett., 42, 883 (1983)

29. V. Zekeriya and T-P. Ma, Appl. Phys. Lett., 47, 54 (1985)

30. F. J. Grunthaner, P. J. Grunthaner, M. H. Hecht, D. Lawson, proceedings of the International Conference on Insulating Films on Semiconductors (INFOS), April 16-18, 1985, Toulouse, France